

Spin-Orbit Synchronization and Singular Perturbation Theory

Clodoaldo Ragazzo · Lucas Ruiz dos Santos

Received: date / Accepted: date

Abstract In this study, we formulate a set of differential equations for a binary system to describe the secular-tidal evolution of orbital elements, rotational dynamics, and deformation (flattening), under the assumption that one body remains spherical while the other is slightly aspherical throughout the analysis. By applying singular perturbation theory, we analyze the dynamics of both the original and secular equations. Our findings indicate that the secular equations serve as a robust approximation for the entire system, often representing a slow-fast dynamical system. Additionally, we explore the geometric aspects of spin-orbit resonance capture, interpreting it as a manifestation of relaxation oscillations within singularly perturbed systems.

Keywords Deformable body · tidal evolution · averaging · spin-orbit resonance · singular perturbation

Preamble

This work is dedicated to the memory of Prof. Jorge Sotomayor, a teacher and friend. Unlike typical mathematical publications, this paper contains no theorems. Instead, it focuses on applications of methods in Ordinary Differential Equations (ODE), a field where, as CR heard from Prof. J. K. Hale, “techniques such as averaging, normal forms, and challenges like the N-body

C. Ragazzo (ORCID 0000-0002-4277-4173)
Instituto de Matemática e Estatística, Universidade de São Paulo, 05508-090 São Paulo, SP, Brazil
E-mail: ragazzo@usp.br

L.S. Ruiz (ORCID 0000-0002-5705-5278)
Instituto de Matemática e Computação, Universidade Federal de Itajubá, 37500-903 Itajubá, MG, Brazil
E-mail: lucasruiz@unifei.edu.br

problem, Hilbert’s XVI problem, and the Lorenz equation, become crucial in research, overshadowing the established general theory.”

CR had the honor of collaborating with Prof. Sotomayor for nearly two decades at the Instituto de Matemática e Estatística da Universidade de São Paulo, where our daily interactions were enriched by his humorous insights on life. More than just a brilliant mathematician, he was vivacious, joyful, and optimistic. He often shared a belief that “for a mathematical field to flourish, it must engage with other sciences or mathematical areas”. Prof. Sotomayor’s work in ODEs, a discipline rooted in Isaac Newton’s efforts to solve physical and geometrical problems, significantly advanced both the theoretical aspects of ODEs through his studies on bifurcations and their practical applications, notably in differential geometry’s lines of curvature.

His students and friends hope that his legacy endures: to approach ODE with joy and happiness.

1 Introduction

The foundations of differential equations trace back to Newton’s pioneering work in mechanics and differential calculus. Newton grounded the law of gravitation mathematically and solved the equations for the motion of two bodies. However, the Newtonian model primarily considers celestial bodies as point masses, a simplification that has its limitations given that celestial entities have finite dimensions.

Planets and substantial satellites exhibit a near-spherical shape. Despite being relatively minuscule compared to their respective diameters, the deformations induced by spin and tidal forces have a considerable impact, instigating significant alterations in both rotation rates and orbits. It is worth noting that all the major satellites within our solar system, including the Moon, operate in a 1:1 spin-orbit resonance (see, e.g., [Murray and Dermott \(2000\)](#)), they complete a single rotation on their axis for every orbit around the planet. Mercury, however, maintains a 3:2 spin-orbit resonance, undergoing three rotations on its axis for every two revolutions around the Sun. Furthermore, a majority of these celestial entities follows elliptical orbits characterized by low eccentricity. Deciphering how this dynamic state was attained, along with determining the associated time scales, holds substantial significance in the scientific realm.

The goal of this study is to introduce equations to describe the perturbative impact of deformations on the motion of two spherical bodies influenced by gravitational interaction. Subsequently, we demonstrate that in certain limiting scenarios, which bear physical relevance, these equations can be analyzed using the mathematical apparatus of singular perturbations.

The earliest and most basic deformation model accounting for energy dissipation was put forth by George Darwin [Darwin \(1879\)](#), son of the renowned biologist Charles Darwin. Darwin built upon previous studies [Thomson \(1863\)](#) concerning the deformation of an elastic, homogeneous, incompressible sphere,

extending the results to address a body constituted of a homogeneous, incompressible, viscous fluid.

Subsequent to Darwin, a significant advancement came with the introduction of Love numbers [Love \(1911\)](#). When the tidal force is decomposed in time via its Fourier components and in space through spherical-harmonic components, the Love number for a specific harmonic frequency and spherical-harmonic mode is a scalar that correlates the amplitude of the tidal force to the deformation's amplitude. Essentially, Love numbers act as functions within the frequency space, offering a phenomenological approach to elucidate force-deformation relationships. Estimates of Love numbers can be derived from observational data.

Over the past 70 years, there has been a prolific output of scientific literature focusing on the tidal effects on the motion of celestial bodies. While it is challenging to encompass the breadth of these studies, we will mention a few we are particularly acquainted with.

Kaula [Kaula \(1964\)](#) evaluated the rate of change of the orbital elements using Love numbers for each harmonic mode (see [Boué and Efroimsky \(2019\)](#) and [Efroimsky \(2012\)](#) for further insights on the work of Kaula). Numerous other scholars have investigated equations accounting for deformations averaged over orbital motion. Some important works in this area are: [Goldreich \(1966\)](#), [Singer \(1968\)](#), [Alexander \(1973\)](#), and [Mignard \(1979\)](#) (low-viscosity scenarios); and [Makarov and Efroimsky \(2013\)](#), [Ferraz-Mello \(2013\)](#), [Correia et al. \(2014\)](#), [Ferraz-Mello \(2015b\)](#), and [Boué et al. \(2016\)](#), [Folonier et al. \(2018\)](#), [Ferraz-Mello \(2019\)](#), [Ferraz-Mello et al. \(2020\)](#), [Ferraz-Mello \(2021\)](#) (low and high-viscosity scenarios).

In this paper, for simplicity while maintaining physical relevance, we make the following assumptions:

- 1) The first body is deformable, nearly spherical at all times;
- 2) The second body, which is the tide-raising body, is a point mass;
- 3) The spin (or rotation vector) of the deformable body remains perpendicular to the orbital plane.

The foundational equations for the orbit and rotation of the extended body are standard. Various equations exist in the literature detailing the deformation of extended bodies. We utilize the equations provided in [Ragazzo and Ruiz \(2017\)](#), without the term accounting for the inertia of deformations [Correia et al. \(2018\)](#).

The reduced and averaged equations we introduce here are not novel. Excluding centrifugal deformations, they match those in [Correia and Valente \(2022\)](#). Our analysis parallels the approach in [Correia et al. \(2014\)](#), Section 5. The primary contributions of this paper include:

- 1) Clearly stating mathematical assumptions used in deriving the averaged and reduced equations;
- 2) Framing the averaged equations as a slow-fast system;
- 3) Beginning a geometric examination of the slow system using numerically generated figures to illustrate the “relaxation jumps”.

We adopt the geometric method set out by Fenichel [Fenichel \(1971\)](#), [Fenichel \(1974\)](#), [Fenichel \(1977\)](#), [Fenichel \(1979\)](#), and [Krupa and Szmolyan \(2001b\)](#) without fully verifying all the assumptions. A comprehensive mathematical analysis of the equations presented may necessitate extensive research.

The paper is structured as follows:

In [Section 2](#), we outline the core equations of the system. We assess the magnitude of various terms and introduce a parameter representing the minor nature of the deformations.

In [Section 3](#), we examine the limit when deformations approach zero, averaging them over orbital motion. This leads to equations with “passive deformations” that do not influence the orbit.

In [Section 4](#), we suggest that for minor deformations, the primary equations possess an attracting invariant manifold matching the deformations from [Section 3](#). This manifold’s existence depends on the body’s rheology. As the body becomes more viscous, the manifold becomes less attractive¹. Given the enhanced spin-orbit coupling at high viscosity, assessing the credibility of our calculations and assumptions in this section presents a compelling mathematical challenge.

In [Section 5](#), we average the orbital and spin equations based on the preceding section’s invariant manifold.

[Section 6](#) reveals that the averaged equations exhibit a slow-fast split. The fast variable is the body’s spin, while the slower variables are orbital eccentricity and the semi-major axis.

In [Section 7](#), we delineate a condition for the folding of the slow manifold and provide a numerical illustration of its geometry. We also present a geometric interpretation of the dynamics within this manifold, emphasizing rapid spin transitions as instances of “relaxation jumps” [Mishchenko \(2013\)](#), [Krupa and Szmolyan \(2001b\)](#).

[Section 8](#) concludes the paper, recapping the pivotal mathematical queries regarding the simplification of the initial equations and the dynamics of the reduced equations.

This paper was written concurrently with a companion paper [Ragazzo and Ruiz \(2024\)](#), which has a more physics-oriented content. The focus of [Ragazzo and Ruiz \(2024\)](#) is on the implications for dynamics of using rheological models more complex than the one employed here.

2 The fundamental equations.

Let m_0 and m represent the masses of two celestial bodies, which could be a planet and a star, or a planet and a satellite, etc. The body with mass m_0 is treated as a point mass, while the body with mass m is always a small

¹ This counterintuitive claim is associated with the omission of deformation inertia. In the equation for the damped harmonic oscillator $m\ddot{x} = -x - \eta\dot{x}$, the solutions converge to zero more rapidly as the damping coefficient η increases. If the inertia coefficient is zero, the equation simplifies to $\eta\dot{x} = -x$, leading to the opposite effect: $x(t) = e^{-t/\eta}x(0)$.

deformation of a spherical body with a moment of inertia I_o . We assume that the deformations do not alter the volume of the body, implying that I_o remains constant, a result attributed to Darwin [Rochester and Smylie \(1974\)](#). Often, we will refer to the bodies simply as the point mass and the body.

For convenience, we write the deviatoric part of the moment of inertia matrix \mathbf{I} in non-dimensional form:

$$\mathbf{I} = I_o(\mathbf{1} - \mathbf{b}) \quad (2.1)$$

where $\mathbf{1}$ is the identity and \mathbf{b} is a symmetric and traceless matrix. We denote matrices and vectors in bold face. The matrix \mathbf{b} is termed the deformation matrix.

Consider an orthonormal frame $\{\mathbf{e}_1, \mathbf{e}_2, \mathbf{e}_3\}$. We assume that the vector \mathbf{x} , from the center of mass of the body to the point mass, lies in the plane spanned by $\{\mathbf{e}_1, \mathbf{e}_2\}$. The angular velocity of the body, $\boldsymbol{\omega}$, is perpendicular to the orbital plane, represented as $\boldsymbol{\omega} = \omega \mathbf{e}_3$. The deformation matrix is given by:

$$\mathbf{b} = \begin{pmatrix} b_{11} & b_{12} & 0 \\ b_{12} & b_{22} & 0 \\ 0 & 0 & b_{33} \end{pmatrix}, \quad \text{with } b_{33} = -b_{11} - b_{22}. \quad (2.2)$$

Under the given assumptions, Newton's equation for the relative position is expressed as:

$$\ddot{\mathbf{x}} = G(m_0 + m) \left\{ -\frac{\mathbf{x}}{|\mathbf{x}|^3} + \frac{I_o}{m} \left(-\frac{15}{2} \frac{1}{|\mathbf{x}|^7} (\mathbf{b}\mathbf{x} \cdot \mathbf{x})\mathbf{x} + 3 \frac{1}{|\mathbf{x}|^5} \mathbf{b}\mathbf{x} \right) \right\}, \quad (2.3)$$

where it is assumed that in the region occupied by the body, the gravitational field of the point mass is accurately represented by its quadrupolar approximation.

The spin angular momentum of the body is denoted by $\boldsymbol{\ell}_s = \ell_s \mathbf{e}_3$, with the index s representing spin, and is defined as:

$$\ell_s = \omega I_o(1 - b_{33}). \quad (2.4)$$

In the context of the quadrupolar approximation, Euler's equation for the variation of ℓ_s is:

$$\dot{\ell}_s = -\frac{3GI_o m_0}{\|\mathbf{x}\|^5} \left\{ x_1 x_2 (b_{22} - b_{11}) + b_{12} (x_1^2 - x_2^2) \right\}. \quad (2.5)$$

For a rigid body, a specific frame exists, known as the body frame, in which the body remains stationary and its angular momentum with respect to this frame is zero. Similarly, for a deformable body, there is an equivalent frame, called the Tisserand frame, where the body's angular momentum is null. The orientation of the Tisserand frame $\mathbf{K} := \{\mathbf{e}_{T1}, \mathbf{e}_{T2}, \mathbf{e}_{T3}\}$ with respect to the inertial frame $\boldsymbol{\kappa} := \{\mathbf{e}_1, \mathbf{e}_2, \mathbf{e}_3\}$ is given by

$$\mathbf{R}(\phi) = \begin{pmatrix} \cos \phi & -\sin \phi & 0 \\ \sin \phi & \cos \phi & 0 \\ 0 & 0 & 1 \end{pmatrix} : \mathbf{K} \rightarrow \boldsymbol{\kappa} \quad (2.6)$$

and by definition, the rate of change of the angle ϕ is given by:

$$\dot{\phi} = \omega. \quad (2.7)$$

To complete the set of equations (2.3) and (2.5), we require additional equations for the deformation matrices. These equations were derived within the Lagrangian formalism and utilizing what was termed the ‘‘Association Principle,’’ as detailed in Ragazzo and Ruiz (2015), Ragazzo and Ruiz (2017) (see, also Gevorgyan et al. (2020) addressing the treatment of Andrade rheology, Ragazzo et al. (2022) extending to bodies with permanent deformation, and Gevorgyan (2021) and Gevorgyan et al. (2023) exploring the relations with the rheology of layered bodies).

To maintain simplicity in mathematical expressions, we consider only the basic rheology of ‘‘Kelvin-Voigt’’ combined with self-gravity here. The exploration of more generalized rheologies, which might introduce new time scales to the problem, is reserved for a companion paper Ragazzo and Ruiz (2024).

The Tisserand frame of the body is the natural frame to present the equations for deformations. In this frame, the deformation matrix and the position vector are denoted by capital letters as follows:

$$\mathbf{B} = \mathbf{R}(\phi)\mathbf{b}\mathbf{R}^{-1}(\phi) \quad \mathbf{X} = \mathbf{R}^{-1}(\phi)\mathbf{x}. \quad (2.8)$$

The governing equation for \mathbf{B} is:

$$\eta\dot{\mathbf{B}} + (\gamma + \alpha)\mathbf{B} = \mathbf{F}, \quad (2.9)$$

where:

- γ , with dimensions of $1/\text{time}^2$, is a parameter representing the self-gravity rigidity of the body; a larger γ indicates a stronger gravitational force holding the body together.
- α , also with dimensions of $1/\text{time}^2$, signifies the elastic rigidity of the body; for a fluid body, $\alpha = 0$.
- η , dimensions of $1/\text{time}$, is a viscosity parameter; a body with a larger η is harder to deform at a given rate compared to a body with a smaller η .
- \mathbf{F} , with dimensions $1/\text{time}^2$, is the force matrix in the Tisserand frame \mathbf{K} :

$$\begin{aligned} \mathbf{F} &:= \mathbf{C} + \mathbf{S} && \text{Deformation force} \\ \mathbf{C} &:= \frac{\omega^2}{3} \begin{pmatrix} 1 & 0 & 0 \\ 0 & 1 & 0 \\ 0 & 0 & -2 \end{pmatrix} && \text{centrifugal force} \\ \mathbf{S} &:= \frac{3Gm_0}{|\mathbf{X}|^5} \left(\mathbf{X} \otimes \mathbf{X} - \frac{|\mathbf{X}|^2}{3} \mathbf{1} \right) && \text{Tidal force} \end{aligned} \quad (2.10)$$

where $\mathbf{X} \otimes \mathbf{X}$ is a matrix with entries $(\mathbf{X} \otimes \mathbf{X})_{ij} = X_i X_j$.

To determine the Love number function associated with the deformation equation (2.9), we consider a simple harmonic force term of the form

$$\mathbf{F}(t) = \widehat{\mathbf{F}} e^{\sigma t}$$

where $\widehat{\mathbf{F}}$ is a complex amplitude matrix, and $\sigma \in \mathbb{R}$ is the constant forcing frequency. Assuming a solution of the form $\mathbf{B}(t) = \widehat{\mathbf{B}} e^{\sigma t}$, we derive the relationship between the complex amplitudes as

$$\widehat{\mathbf{B}} = \underbrace{\frac{1}{\gamma + \alpha + i\eta\sigma}}_{C(\sigma)} \widehat{\mathbf{F}} = \left(\frac{1}{\gamma + \alpha} \right) \frac{1}{1 + i\tau\sigma} \widehat{\mathbf{F}} = \left(\frac{1}{\gamma + \alpha} \right) \frac{1 - i\tau\sigma}{1 + \tau^2\sigma^2} \widehat{\mathbf{F}} \quad (2.11)$$

where $C(\sigma)$ is the complex compliance and

$$\tau := \frac{\eta}{\gamma + \alpha} \quad \text{represents the time constant.} \quad (2.12)$$

The complex Love number $k_2(\sigma)$, commonly defined differently (see, e.g., [Ragazzo and Ruiz \(2017\)](#)), is proportional to the complex compliance $C(\sigma)$ as outlined in [Mathews et al. \(2002\)](#) (paragraph 21):

$$k_2(\sigma) = \frac{3GI_o}{R^5} C(\sigma) = \left(\frac{3GI_o}{R^5} \frac{1}{\gamma + \alpha} \right) \frac{1 - i\tau\sigma}{1 + \tau^2\sigma^2} = k_o \frac{1 - i\tau\sigma}{1 + \tau^2\sigma^2}, \quad (2.13)$$

where the number $k_o := \frac{3GI_o}{R^5} \frac{1}{\gamma + \alpha}$ denotes the secular Love number, representing the value of $k_2(\sigma)$ for static forces ($\sigma = 0$).

In the case of a fluid body, the elastic modulus α is zero, and

$$k_o = k_f := \frac{3GI_o}{R^5} \frac{1}{\gamma} \quad \text{fluid Love number.} \quad (2.14)$$

The body is held together solely by self-gravity. For a homogeneous fluid body of any density, $k_f = 3/2$. As discussed in [Ragazzo \(2020\)](#), this represents the maximum possible value of k_f when the density of the body increases towards the center. Given that for any non-null elastic rigidity $\alpha > 0$, $k_f > k_o$, we conclude that for any stably stratified body,

$$k_o = \frac{3GI_o}{R^5} \frac{1}{\gamma + \alpha} \leq \frac{3}{2}. \quad (2.15)$$

Historical note. Darwin was the pioneer in deriving equation (2.13), while examining tides on a homogeneous body composed of viscous fluid. In page 13 of [Darwin \(1879\)](#), Darwin stated: ‘‘Thus we see that the tides of the viscous sphere are the equilibrium tides of a fluid sphere as $\cos \epsilon : 1$, and that there is a retardation time $\frac{\epsilon}{\sigma}$ ’’. In his paper, ν denotes fluid viscosity, and $\tan \epsilon = \frac{19}{2} \frac{\nu}{gR\rho} \sigma$, where g represents surface gravity, and ρ is the mass per unit volume of the body.

Given that for a homogeneous fluid body $k_o = k_f = 3/2$, Darwin's statement can be reformulated as

$$k_2 = \frac{3}{2} \cos \epsilon e^{-i\epsilon} = \frac{3}{2} \frac{1}{\sqrt{1 + \tan^2 \epsilon}} e^{-i\epsilon} = \frac{3}{2} \frac{1}{\sqrt{1 + \tau^2 \sigma^2}} e^{-i\epsilon} = \frac{3}{2} \frac{1}{1 + i\tau\sigma},$$

where

$$\tan \epsilon = \tau\sigma \quad \text{and} \quad \tau = \frac{19}{2} \frac{\nu}{gR\rho}. \quad (2.16)$$

Utilizing the relationships for a homogeneous spherical body, $I_o = \frac{2}{5}mR^2$, $g = \frac{Gm}{R^2}$, and $\rho = m/\frac{4\pi R^3}{3}$, where m is the mass and R is the radius of the fluid body, and from the relations $k_o = k_f = \frac{3}{2} = \frac{3I_o G}{R^5} \frac{1}{\gamma}$ and $\tau = \frac{\eta}{\gamma} = \frac{19}{2} \frac{\nu}{gR\rho}$, we deduce

$$\eta = \frac{152\pi}{15} \frac{R}{m} \nu, \quad (2.17)$$

which aligns with a relation in (Correia et al., 2018, Eq. (39)).

The theory developed by Darwin (1879), Darwin (1880) has predominantly been applied in the frequency domain. Influenced by Darwin's work, Ferraz-Mello (2013) formulated an equation for the motion of the surface of the body under tidal forcing in the time domain. When $\alpha = 0$, the model in Correia et al. (2014) with $\tau_e = 0$, the model in Ferraz-Mello (2013), and equation (2.9) are all equivalent (our τ corresponds to the τ in Correia et al. (2014), which is equal to the parameter "1/ γ " used in Ferraz-Mello (2013)). See Correia et al. (2014), paragraph above equation (90), and Ferraz-Mello (2015a) for the equivalence between the models in Ferraz-Mello (2013) and Correia et al. (2014).

3 Zero deformation limit.

In numerous celestial mechanics problems, bodies maintain near-spherical shapes at all times, which can be reformulated as

$$\|\mathbf{B}\| \ll 1, \quad \text{where} \quad \|\mathbf{B}\|^2 = \frac{1}{2} \sum_{ij} B_{ij}^2. \quad (3.18)$$

Given that equation (2.9) for \mathbf{B} is linear, $\|\mathbf{B}\|$ is small if, and only if, $\|\mathbf{F}\|$ is small.

The relative motion between two nearly spherical bodies approximates Keplerian motion. Let a , n , and e represent the semi-major axis, the mean motion (period/(2π)), and the eccentricity of the Keplerian ellipses, respectively. The magnitude of the force terms in the deformation equation (2.9) is proportional to the following characteristic frequencies:

$$\begin{aligned} \mathbf{S} &= \frac{3Gm_0}{|\mathbf{x}|^5} \left(\mathbf{x} \otimes \mathbf{x} - \frac{|\mathbf{x}|^2}{3} \mathbf{1} \right) \approx \frac{Gm_0}{a^3} = \frac{m_0}{m + m_0} n^2 \quad \text{tidal force;} \\ \mathbf{C} &= - \left(\boldsymbol{\omega}_\alpha \otimes \boldsymbol{\omega}_\alpha - \frac{\|\boldsymbol{\omega}_\alpha\|^2}{3} \mathbf{1} \right) \approx 2\omega^2 \quad \text{centrifugal force.} \end{aligned} \quad (3.19)$$

The forces on the right-hand side of equation (2.9) are counteracted by the body's self-gravity and possibly elastic rigidity $\alpha \geq 0$. The static deformations are then given by

$$\mathbf{B} = \frac{\mathbf{C}}{\gamma + \alpha} + \frac{\mathbf{S}}{\gamma + \alpha} = k_o \frac{R^5}{3G I_o} (\mathbf{C} + \mathbf{S}),$$

where we used $k_o := \frac{3GI_o}{R^5} \frac{1}{\gamma + \alpha}$.

The order of magnitudes in equation (3.19) and inequality (2.15) imply

$$\|\mathbf{B}\| \leq \frac{R^5 \omega^2}{GI_o} + \frac{m_0 R^5}{2a^3 I_o}. \quad (3.20)$$

This indicates that the region in phase space defined by the following inequalities:

$$\zeta_c := \frac{R^5 \omega^2}{GI_o} \ll 1 \quad \text{and} \quad \zeta_T := \frac{m_0 R^5}{2I_o a^3} \ll 1 \quad (3.21)$$

adheres to the small deformation hypothesis.

3.1 The Zero Deformation Limit

Define the compliance ϵ_d , where d denotes deformation, as follows:

$$\epsilon_d := \frac{1}{\gamma + \alpha} \quad \text{dimension of time}^2. \quad (3.22)$$

We then express

$$\mathbf{B} = \epsilon_d \tilde{\mathbf{B}} \quad (3.23)$$

and substitute into equations (2.3), (2.4), (2.5), and (2.9) to yield

$$\begin{aligned} \ddot{\mathbf{x}} &= G(m_0 + m) \left\{ -\frac{\mathbf{x}}{|\mathbf{x}|^3} + \epsilon_d \frac{I_o}{m} \left(-\frac{15}{2} \frac{1}{|x|^7} (\tilde{\mathbf{b}}\mathbf{x} \cdot \mathbf{x})\mathbf{x} + 3 \frac{1}{|\mathbf{x}|^5} \tilde{\mathbf{b}}\mathbf{x} \right) \right\} \\ \dot{\ell}_s &= -\epsilon_d \frac{3GI_o m_0}{\|\mathbf{x}\|^5} \left\{ x_1 x_2 (\tilde{b}_{22} - \tilde{b}_{11}) + \tilde{b}_{12} (x_1^2 - x_2^2) \right\} \\ \ell_s &= \omega I_o (1 - \epsilon_d \tilde{b}_{33}) \\ \tau \dot{\tilde{\mathbf{B}}} + \tilde{\mathbf{B}} &= \mathbf{F} \end{aligned} \quad (3.24)$$

where τ is defined in (2.12) and $\tilde{\mathbf{b}} = \mathbf{R}(\phi) \tilde{\mathbf{B}} \mathbf{R}^{-1}(\phi)$.

The zero deformation limit is defined by:

$$\epsilon_d = \frac{1}{\gamma + \alpha} \rightarrow 0 \quad \text{while} \quad \tau = \frac{\eta}{\alpha + \gamma} \text{ remains constant.} \quad (3.25)$$

In the zero deformation limit, equation (3.24) simplifies to:

$$\begin{aligned} \ddot{\mathbf{x}} &= -G(m_0 + m) \frac{\mathbf{x}}{|\mathbf{x}|^3} \\ \dot{\ell}_s &= \dot{\omega} I_o = 0 \\ \tau \dot{\tilde{\mathbf{B}}} + \tilde{\mathbf{B}} &= \mathbf{F} \end{aligned} \quad (3.26)$$

In this scenario, the body spin, ω , remains constant and \mathbf{x} follows a Keplerian ellipse.

To describe the Keplerian orbits, we change from variables $(\mathbf{x}, \dot{\mathbf{x}})$ to $\ell \in \mathbb{R}$ (orbital angular momentum), \mathbf{A} (the Laplace vector), and f (the true anomaly), defined as:

$$\begin{aligned} \ell \mathbf{e}_3 &= \boldsymbol{\ell} = \mu \mathbf{x} \times \dot{\mathbf{x}} \quad \text{orbital angular momentum} \\ \mathbf{A} &= \frac{1}{c} \dot{\mathbf{x}} \times \boldsymbol{\ell} - \frac{\mathbf{x}}{|\mathbf{x}|} \quad \text{Laplace vector} \end{aligned} \quad (3.27)$$

where

$$\mu = \frac{m_0 m}{m_0 + m} = \text{reduced mass}, \quad c = G m m_0. \quad (3.28)$$

The Laplace vector is normalized such that $\|\mathbf{A}\| = e$ is the orbital eccentricity and it points towards the periapsis, where $\|\mathbf{x}\|$ is minimized.

The three vectors

$$\mathbf{e}_A := \frac{\mathbf{A}}{\|\mathbf{A}\|}, \quad \mathbf{e}_H := \mathbf{e}_3 \times \mathbf{e}_A, \quad \mathbf{e}_3 \quad (3.29)$$

constitute an orthonormal basis, expressed in terms of the inertial frame basis vectors as

$$\mathbf{e}_A := \cos \varpi \mathbf{e}_1 + \sin \varpi \mathbf{e}_2, \quad \mathbf{e}_H := -\sin \varpi \mathbf{e}_1 + \cos \varpi \mathbf{e}_2. \quad (3.30)$$

Here, ϖ denotes the longitude of the periapsis, the angle between \mathbf{e}_A and \mathbf{e}_1 .

The orbit is represented by

$$\begin{aligned} \mathbf{x} &= r \mathbf{R}(f + \varpi) \mathbf{e}_1 = r(\cos(f + \varpi) \mathbf{e}_1 + \sin(f + \varpi) \mathbf{e}_2) \\ &= r(\cos f \mathbf{e}_A + \sin f \mathbf{e}_H), \end{aligned} \quad (3.31)$$

where \mathbf{R} is the rotation matrix about the axis \mathbf{e}_3 , as given in equation (2.6), and $r(t) = \|\mathbf{x}(t)\|$.

3.2 Passive deformations.

The equations at the zero deformation limit (3.26) in the new variables become (see, e.g., Murray and Dermott (2000) for details):

$$\begin{aligned} \dot{\mathbf{A}} &= 0 \\ \dot{\ell} &= 0 \\ \dot{f} &= \frac{\mu \ell}{r^2}, \quad \text{where } r = \frac{a(1 - e^2)}{1 + e \cos f} = \frac{\ell^2}{\mu c} \frac{1}{1 + e \cos f} \\ \dot{\omega} &= 0 \\ \tau \dot{\tilde{\mathbf{B}}} + \tilde{\mathbf{B}} &= \mathbf{C} + \mathbf{S} \end{aligned} \quad (3.32)$$

where \mathbf{C} and \mathbf{S} are given in equation (2.10).

In order to write \mathbf{S} in a convenient way, we define the matrices

$$\mathbf{Y}_{-2} := \frac{1}{\sqrt{2}} \begin{pmatrix} 1 & i & 0 \\ i & -1 & 0 \\ 0 & 0 & 0 \end{pmatrix} \quad \mathbf{Y}_0 := \frac{1}{\sqrt{3}} \begin{pmatrix} 1 & 0 & 0 \\ 0 & 1 & 0 \\ 0 & 0 & -2 \end{pmatrix} \quad \mathbf{Y}_2 := \frac{1}{\sqrt{2}} \begin{pmatrix} 1 & -i & 0 \\ -i & -1 & 0 \\ 0 & 0 & 0 \end{pmatrix}, \quad (3.33)$$

with $\mathbf{Y}_{-2} = \overline{\mathbf{Y}}_2$, where the overline represents complex conjugation. These matrices have a simple transformation rule with respect to rotations about the axis \mathbf{e}_3 , namely

$$\mathbf{R}(\theta)\mathbf{Y}_j\mathbf{R}^{-1}(\theta) = e^{ij\theta} \mathbf{Y}_j, \quad j = -2, 0, 2. \quad (3.34)$$

Using

$$\begin{aligned} \mathbf{X} &= \mathbf{R}^{-1}(\phi)\mathbf{x} = r\mathbf{R}(f + \varpi - \phi)\mathbf{e}_1 \\ &= r(\cos(f + \varpi - \phi)\mathbf{e}_1 + \sin(f + \varpi - \phi)\mathbf{e}_2), \end{aligned} \quad (3.35)$$

the tidal-force matrix in equation (2.10) can be written as

$$\mathbf{S} = \frac{3Gm_0}{r^3} \mathbf{R}(f + \varpi - \phi) \left(\mathbf{e}_1 \otimes \mathbf{e}_1 - \frac{1}{3} \mathbf{1} \right) \mathbf{R}^{-1}(f + \varpi - \phi). \quad (3.36)$$

In the basis $\{\mathbf{Y}_{-2}, \mathbf{Y}_0, \mathbf{Y}_2\}$

$$\mathbf{e}_1 \otimes \mathbf{e}_1 - \frac{1}{3} \mathbf{1} = \frac{1}{2} \left\{ \frac{\mathbf{Y}_{-2}}{\sqrt{2}} + \frac{\mathbf{Y}_0}{\sqrt{3}} + \frac{\mathbf{Y}_2}{\sqrt{2}} \right\} \quad (3.37)$$

that implies

$$\begin{aligned} \mathbf{S} &= \frac{3Gm_0}{r^3} \mathbf{R}_3(f + \varpi - \phi) \left\{ \mathbf{e}_1 \otimes \mathbf{e}_1 - \frac{1}{3} \mathbf{1} \right\} \mathbf{R}_3^{-1}(f + \varpi - \phi) \\ &= \frac{3Gm_0}{2r^3} \left\{ e^{-2i(f+\varpi-\phi)} \frac{\mathbf{Y}_{-2}}{\sqrt{2}} + \frac{\mathbf{Y}_0}{\sqrt{3}} + e^{2i(f+\varpi-\phi)} \frac{\mathbf{Y}_2}{\sqrt{2}} \right\}. \end{aligned} \quad (3.38)$$

In equation (3.38), the variables r , f , and $\phi = \omega t$ are dependent on t .

To solve the equation $\tau \dot{\tilde{\mathbf{B}}} + \tilde{\mathbf{B}} = \mathbf{C} + \mathbf{S}$, we do a harmonic analysis of the tidal force in equation (3.38) using:

$$\left(\frac{r}{a} \right)^{n'} e^{imf} = \sum_{k=-\infty}^{\infty} X_k^{n',m}(e) e^{ikM}, \quad (3.39)$$

where M denotes the mean anomaly, $\dot{M} = n$, and $X_k^{n',m}(e)$ is termed the Hansen coefficient.

Equations (3.38) and (3.39) imply:

$$\mathbf{S} = \frac{3Gm_0}{2a^3} \sum_{l=-2}^2 \sum_{k=-\infty}^{\infty} e^{i\{t(kn-l\omega)+l\varpi\}} \mathbf{Y}_l U_{kl} \quad (3.40)$$

where $U_{k,-1} = U_{k,1} = 0$ and

$$U_{k,-2} = \frac{X_k^{-3,-2}}{\sqrt{2}}, \quad U_{k0} = \frac{X_k^{-3,0}}{\sqrt{3}}, \quad U_{k2} = \frac{X_k^{-3,2}}{\sqrt{2}}. \quad (3.41)$$

The symmetry property $X_{-k}^{n',-m} = X_k^{n',m}$ implies

$$U_{kj} = U_{-k,-j}. \quad (3.42)$$

The centrifugal force in equation (2.10) can be represented as

$$\mathbf{C} = \frac{\omega^2}{\sqrt{3}} \mathbf{Y}_0. \quad (3.43)$$

To obtain the almost periodic solution of the deformation equation

$$\tau \dot{\tilde{\mathbf{B}}} + \tilde{\mathbf{B}} = \mathbf{C} + \mathbf{S}, \quad (3.44)$$

solving for each Fourier mode separately suffices. An alternative approach involves using the variation of constants formula:

$$\begin{aligned} \tilde{\mathbf{B}}(t) &= \mathbf{B}_d(t) := \int_{-\infty}^0 \frac{e^{s/\tau}}{\tau} \frac{\mathbf{C} + \mathbf{S}(t+s)}{\gamma + \alpha} ds = \frac{\mathbf{C}}{\gamma + \alpha} \\ &+ \frac{3Gm_0}{2a^3} \sum_{l=-2}^2 \sum_{k=-\infty}^{\infty} e^{i\{t(kn-l\omega)+l\varpi\}} \frac{1}{(\gamma + \alpha)(1 + i(kn - l\omega))} \mathbf{Y}_l U_{kl} \\ &= k_\circ \frac{R^5 \omega^2}{G I_\circ} \frac{\mathbf{Y}_0}{3\sqrt{3}} + \frac{m_0 R^5}{2 I_\circ a^3} \sum_{l=-2}^2 \sum_{k=-\infty}^{\infty} e^{i\{t(kn-l\omega)+l\varpi\}} k_2(kn - l\omega) \mathbf{Y}_l U_{kl} \\ &= k_\circ \zeta_c \frac{\mathbf{Y}_0}{3\sqrt{3}} + \zeta_\tau \sum_{l=-2}^2 \sum_{k=-\infty}^{\infty} e^{i\{t(kn-l\omega)+l\varpi\}} k_2(kn - l\omega) \mathbf{Y}_l U_{kl}. \end{aligned} \quad (3.45)$$

Here, the definitions of the Love number k_2 and the secular Love number k_\circ from equation (2.13) are used as well as the definitions of ζ_c and ζ_τ from equation (3.21).

Given that

$$\int_{-\infty}^0 \frac{e^{s/\tau}}{\tau} ds = 1,$$

this formula indicates that the almost periodic solution of the tide equation is a time-averaged tidal force with an exponential weight decaying towards the past, characterized by time τ . Note that when $\tau > 0$ is nearly zero, integration by parts of the right-hand side of equation (3.45) yields

$$\mathbf{B}_d(t) - k_\circ \zeta_c \frac{\mathbf{Y}_0}{3\sqrt{3}} \approx \frac{\mathbf{S}(t)}{\gamma + \alpha} - \tau \frac{\dot{\mathbf{S}}(t)}{\gamma + \alpha} \approx \frac{\mathbf{S}(t - \tau)}{\gamma + \alpha}. \quad (3.46)$$

This represents the usual time delay approximation with corrections of the order of τ^2 .

The limit case of $\tau \rightarrow \infty$ also presents interest. Here, we can interpret the averaging in equation (3.45) as approximately the ordinary averaging

$$\lim_{\tau \rightarrow \infty} \frac{1}{\tau} \int_{-\tau}^0 \frac{\mathbf{S}}{\gamma + \alpha} ds.$$

4 Deformation Manifold.

The function $t \rightarrow \mathbf{B}_d$ provides a solution to the deformation equation (3.44) only when $\epsilon_d = 0$. To analyze the case where $\epsilon_d > 0$, we introduce new deformation variables $\delta\mathbf{B}$:

$$\tilde{\mathbf{B}} = \mathbf{B}_d + \delta\mathbf{B}, \quad (4.47)$$

and using these variables we write equation (3.24)

$$\begin{aligned} \ddot{\mathbf{x}} &= G(m_0 + m) \left\{ -\frac{\mathbf{x}}{|\mathbf{x}|^3} + \epsilon_d \frac{I_o}{m} \left(-\frac{15}{2} \frac{1}{|x|^7} (\tilde{\mathbf{b}}\mathbf{x} \cdot \mathbf{x})\mathbf{x} + 3 \frac{1}{|\mathbf{x}|^5} \tilde{\mathbf{b}}\mathbf{x} \right) \right\} \\ \dot{\ell}_s &= -\epsilon_d \frac{3GI_o m_0}{\|\mathbf{x}\|^5} \left\{ x_1 x_2 (\tilde{b}_{22} - \tilde{b}_{11}) + \tilde{b}_{12} (x_1^2 - x_2^2) \right\} \\ \ell_s &= \omega I_o (1 - \epsilon_d \tilde{b}_{33}) \\ \tau \delta \dot{\mathbf{B}} + \delta \mathbf{B} &= \mathcal{O}(\epsilon_d). \end{aligned} \quad (4.48)$$

For $\epsilon_d = 0$, equation (3.26) possesses the invariant manifold:

$$\Sigma_0 := \{\delta\mathbf{B} = 0\}. \quad (4.49)$$

The variables $\delta\mathbf{B}$ are transversal to Σ_0 , and all associated eigenvalues equal $-1/\tau < 0$. Given this, a theorem by Fenichel (Fenichel, 1971, Theorem 3) suggests that for sufficiently small ϵ_d , there is an invariant manifold represented as a graph:

$$\Sigma_{\epsilon_d} := \left\{ (\mathbf{x}, \dot{\mathbf{x}}, \ell_s, \epsilon_d) \rightarrow \delta\mathbf{B} \right\}. \quad (4.50)$$

Additionally, Σ_{ϵ_d} approximates Σ_0 to order ϵ_d , as visualized in Figure 1. The vector field on Σ_{ϵ_d} , considering corrections of order ϵ_d , is derived from equations (4.48) by ignoring the variables $\delta\mathbf{B}$ and setting $\tilde{\mathbf{B}} = \mathbf{B}_d$ in the equations for $\dot{\mathbf{x}}$ and ℓ . Thus, the equation on Σ_{ϵ_d} is:

$$\begin{aligned} \ddot{\mathbf{x}} &= G(m_0 + m) \left\{ -\frac{\mathbf{x}}{|\mathbf{x}|^3} + \epsilon_d \frac{I_o}{m} \left(-\frac{15}{2} \frac{1}{|x|^7} (\mathbf{b}_d \mathbf{x} \cdot \mathbf{x})\mathbf{x} + 3 \frac{1}{|\mathbf{x}|^5} \mathbf{b}_d \mathbf{x} \right) \right\} \\ \dot{\ell}_s &= -\epsilon_d \frac{3GI_o m_0}{\|\mathbf{x}\|^5} \left\{ x_1 x_2 (b_{d22} - b_{d11}) + b_{d12} (x_1^2 - x_2^2) \right\} \\ \ell_s &= \omega I_o (1 - \epsilon_d b_{d33}), \end{aligned} \quad (4.51)$$

where, $\mathbf{b}_d = \mathbf{R}(\phi) \mathbf{B}_d \mathbf{R}^{-1}(\phi)$.

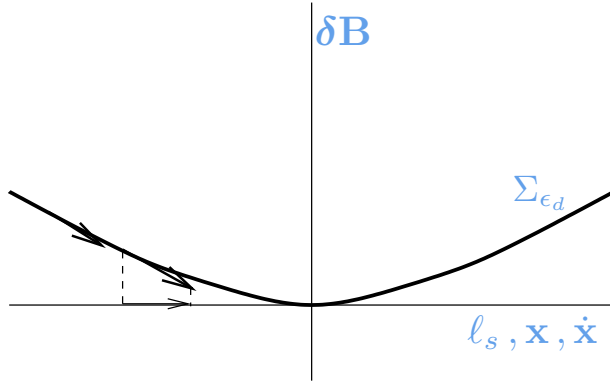


Fig. 1 Illustration of the Deformation Invariant Manifold $\Sigma_{\epsilon_d} := \{(\mathbf{x}, \dot{\mathbf{x}}, \ell_s, \epsilon_d) \rightarrow \delta \mathbf{B}\}$. With the parameterization defined by $(\mathbf{x}, \dot{\mathbf{x}}, \ell_s, \epsilon_d)$, the vector field on Σ_{ϵ_d} follows from (4.51).

The Fenichel theorem requires a specific condition concerning the eigenvalues of the linear equation: they must be sufficiently distant from the imaginary axis, depending on the flow on Σ_0 , which is fulfilled in this case since they are constant.

When n and ω are neither small, to ensure the validity of the averaging, nor excessively large, which would violate inequalities (3.21) and result in large deformations, the approximation of Σ_0 by Σ_{ϵ_d} remains accurate. Under these conditions, changes in the Keplerian elements and spin are gradual, allowing the body ample time to adjust. The body maintains an average shape consistent with its secular Love number; for $\alpha = 0$, it remains in hydrostatic equilibrium, countering centrifugal forces and slow tides.

An intriguing scenario arises when either $\tau n \gg 1$ or $\tau \omega \gg 1$. Here, the body lacks the time to relax amid orbital and spin modifications, causing the deformation to retain a memory of a past initial state. In such situations, Fenichel's theorem is not applicable. If $\tau \gg 1$ and the initial condition is $\tilde{\mathbf{B}} = \tilde{\mathbf{B}}_o$, the solution to the homogeneous equation $\tau \dot{\tilde{\mathbf{B}}} + \tilde{\mathbf{B}} = 0$ decays slowly as

$$\tilde{\mathbf{B}}(t) = \tilde{\mathbf{B}}_o e^{-t/\tau}. \quad (4.52)$$

In Ragazzo et al. (2022), in a situation similar to this one, we added a permanent deformation $\tilde{\mathbf{B}}_o$ to \mathbf{B}_d and continued. Adopting the same approach here is feasible, even without a mathematical basis. However, we must separate the orbital motion's averaging into two components: one for terms with \mathbf{B}_d and another for terms with $\tilde{\mathbf{B}}_o$. The averaging of terms associated with $\tilde{\mathbf{B}}_o$ would resemble the averaging in rigid body problems. Here, we will not introduce the permanent deformation to keep the following analysis as simple as possible.

Later in this paper, we'll explore situations where τn is large, assuming that, despite its size, Fenichel's conditions remain met. This assumption war-

rants further mathematical scrutiny, potentially through multi-timescale system theories.

5 Orbital Averaging

We average equation (4.51) with respect to orbital motion. We set the scaling parameter ϵ_d to 1. Equations (4.51) and (3.45) then become:

$$\begin{aligned}\ddot{\mathbf{x}} &= G(m_0 + m) \left\{ -\frac{\mathbf{x}}{|\mathbf{x}|^3} + \frac{\mathbf{I}_o}{m} \left(-\frac{15}{2} \frac{1}{|\mathbf{x}|^7} (\mathbf{b}_d \mathbf{x} \cdot \mathbf{x}) \mathbf{x} + 3 \frac{1}{|\mathbf{x}|^5} \mathbf{b}_d \mathbf{x} \right) \right\}, \\ \dot{\ell}_s &= -\frac{3G\mathbf{I}_o m_0}{\|\mathbf{x}\|^5} \{x_1 x_2 (b_{d22} - b_{d11}) + b_{d12} (x_1^2 - x_2^2)\}, \\ \ell_s &= \omega \mathbf{I}_o (1 - b_{d33}), \\ \mathbf{b}_d &= k_o \zeta_c \frac{\mathbf{Y}_0}{3\sqrt{3}} + \zeta_T \sum_{l=-2}^2 \sum_{k=-\infty}^{\infty} e^{i\{tkn+l\varpi\}} k_2(kn - l\omega) \mathbf{Y}_l U_{kl}.\end{aligned}\tag{5.53}$$

Using variables ℓ , \mathbf{A} , and f defined in equations (3.27) and (3.28), equation (5.53) transforms to:

$$\begin{aligned}\dot{\ell}_s &= -3c \frac{\mathbf{I}_o}{m} E_1, \\ \dot{\ell} &= 3c \frac{\mathbf{I}_o}{m} E_1, \\ \ell_s &= \omega \mathbf{I}_o (1 - \langle b_{d33} \rangle), \\ \dot{\mathbf{A}} &= 3 \frac{\ell}{\mu} \frac{\mathbf{I}_o}{m} \left(-\frac{5}{2} \mathbf{E}_2 + \mathbf{E}_3 \right) \times \mathbf{e}_3 + 3 \frac{c}{\ell} \frac{\mathbf{I}_o}{m} \mathbf{E}_4 + 3 \frac{c}{\ell} \frac{\mathbf{I}_o}{m} E_1 \mathbf{A}.\end{aligned}\tag{5.54}$$

The terms requiring averaging are:

$$\begin{aligned}E_1 &= \left\langle \frac{x_1 x_2 (b_{d22} - b_{d11}) + b_{d12} (x_1^2 - x_2^2)}{\|\mathbf{x}\|^5} \right\rangle, \\ \mathbf{E}_2 &= \left\langle \frac{1}{|\mathbf{x}|^7} (\mathbf{b}_d \mathbf{x} \cdot \mathbf{x}) \mathbf{x} \right\rangle, \\ \mathbf{E}_3 &= \left\langle \frac{1}{|\mathbf{x}|^5} \mathbf{b}_d \mathbf{x} \right\rangle, \\ \mathbf{E}_4 &= \left\langle \frac{1}{|\mathbf{x}|^5} \left((\mathbf{x} \times \mathbf{b}_d \mathbf{x}) \cdot \mathbf{e}_3 \right) \frac{\mathbf{x}}{|\mathbf{x}|} \right\rangle, \\ \langle b_{d33} \rangle &= \left\langle k_o \zeta_c \frac{\mathbf{e}_3 \cdot \mathbf{Y}_0 \mathbf{e}_3}{3\sqrt{3}} + \zeta_T \sum_{k=-\infty}^{\infty} e^{itkn} k_2(kn) U_{k0} (\mathbf{e}_3 \cdot \mathbf{Y}_0 \mathbf{e}_3) \right\rangle,\end{aligned}\tag{5.55}$$

where $\langle h \rangle = \frac{1}{2\pi} \int_0^{2\pi} h(M) dM$ represents the average over the mean anomaly.

The total angular momentum is conserved and given by:

$$\ell_T := \ell + \ell_s.\tag{5.56}$$

The averaged result yields:

The term E_1 :

$$\begin{aligned}
E_1 &= \left\langle \frac{x_1 x_2 (b_{d22} - b_{d11}) + b_{d12} (x_1^2 - x_2^2)}{\|\mathbf{x}\|^5} \right\rangle \\
&= \sum_{k=-\infty}^{\infty} \frac{i\zeta_T \left(X_k^{-3,-2} X_{-k}^{-3,2} k_2(kn + 2\omega) - X_{-k}^{-3,-2} X_k^{-3,2} k_2(kn - 2\omega) \right)}{2a^3} \\
&= \frac{i\zeta_T}{2a^3} \sum_{k=-\infty}^{\infty} X_k^{-3,2} X_k^{-3,2} (k_2(-kn + 2\omega) - k_2(kn - 2\omega)) \\
&= \frac{\zeta_T}{a^3} \sum_{k=-\infty}^{\infty} \left(X_k^{-3,2}(e) \right)^2 \text{Im } k_2(kn - 2\omega)
\end{aligned}$$

where we used, from equation (2.13), that $k_2(-\sigma)$ is the complex conjugate of $k_2(\sigma)$, represented as $\overline{k_2(\sigma)}$.

We write E_1 as

$$E_1 = \frac{\zeta_T}{a^3} \mathcal{A}_0, \quad \mathcal{A}_0 = \sum_{k=-\infty}^{\infty} \left(X_k^{-3,2}(e) \right)^2 \text{Im } k_2(kn - 2\omega). \quad (5.57)$$

The terms $(-\frac{5}{2}\mathbf{E}_2 + \mathbf{E}_3)$: The calculation of these terms resembles that of E_1 . The analysis was extended and performed using the software ‘‘Mathematica’’. We will skip the detailed steps. The outcomes are:

$$\mathcal{A}_1 = - \sum_k (X_k^{-4,1} + 5X_k^{-4,3}) X_k^{-3,2} \text{Re } k_2(nk - 2\omega) + 2X_k^{-4,1} X_k^{-3,0} \text{Re } k_2(nk) \quad (5.58)$$

$$\mathcal{A}_2 = \sum_k (5X_k^{-4,3} - X_k^{-4,1}) X_k^{-3,2} \text{Im } k_2(kn - 2\omega) + 2X_k^{-4,1} X_k^{-3,0} \text{Im } k_2(nk) \quad (5.59)$$

$$\mathcal{A}_3 = X_0^{-4,1} \quad (5.60)$$

and

$$\begin{aligned}
\left(\begin{array}{c} -\frac{5}{2}\mathbf{E}_2 + \mathbf{E}_3 \\ -\frac{5}{2}\mathbf{E}_2 + \mathbf{E}_3 \end{array} \right)_1 &= \left\{ \frac{\zeta_T}{4a^4} \begin{pmatrix} \mathcal{A}_1 & -\mathcal{A}_2 \\ \mathcal{A}_2 & \mathcal{A}_1 \end{pmatrix} - \frac{k_o \zeta_c}{6a^4} \mathcal{A}_3 \right\} \begin{pmatrix} \cos \varpi \\ \sin \varpi \end{pmatrix} \\
&= \left\{ \frac{\zeta_T}{4a^4} \mathcal{A}_1 - \frac{k_o \zeta_c}{6a^4} \mathcal{A}_3 \right\} \mathbf{e}_A + \frac{\zeta_T}{4a^4} \mathcal{A}_2 \mathbf{e}_H,
\end{aligned} \quad (5.61)$$

where we used equations (3.30).

The term \mathbf{E}_4 : Detailed steps are omitted as before. The outcomes are:

$$\mathcal{A}_4 = \sum_k X_k^{-3,2} (X_k^{-3,1} + X_k^{-3,3}) \text{Im } k_2 (kn - 2\omega) \quad (5.62)$$

$$\mathcal{A}_5 = \sum_k (X_k^{-3,3} - X_k^{-3,1}) X_k^{-3,2} \text{Re } k_2 (kn - 2\omega) \quad (5.63)$$

and

$$\mathbf{E}_4 = \begin{pmatrix} \mathbf{E}_4 \cdot \mathbf{e}_1 \\ \mathbf{E}_4 \cdot \mathbf{e}_2 \end{pmatrix} = \frac{\zeta_T}{2a^3} (\mathcal{A}_4 \mathbf{e}_A + \mathcal{A}_5 \mathbf{e}_H). \quad (5.64)$$

The term $\langle b_{d33} \rangle$:

$$\begin{aligned} \langle b_{d33} \rangle &= \left\langle k_o \zeta_c \frac{\mathbf{e}_3 \cdot \mathbf{Y}_0 \mathbf{e}_3}{3\sqrt{3}} + \zeta_T \sum_{k=-\infty}^{\infty} e^{itkn} k_2(kn) U_{k0}(\mathbf{e}_3 \cdot \mathbf{Y}_0 \mathbf{e}_3) \right\rangle \\ &= -\frac{2}{3} k_o \left(\frac{\zeta_c}{3} + \frac{\zeta_T}{(1-e^2)^{3/2}} \right) \end{aligned} \quad (5.65)$$

where we used that $X_0^{-3,0} = (1-e^2)^{-3/2}$ [Laskar and Boué \(2010\)²](#).

For the Kepler problem, the following relations hold:

$$\ell^2 = \mu c a (1 - e^2) \Rightarrow (1 - e^2) = \frac{\ell^2}{\mu c a}. \quad (5.67)$$

Assuming $\ell > 0$, we can use $G(m_0 + m) = n^2 a^3$ to write:

$$\frac{\ell}{\mu a^2} = n \sqrt{1 - e^2}. \quad (5.68)$$

Using the above relations, further calculations yield:

$$\begin{aligned} \dot{\mathbf{A}} &= \frac{3c}{2\ell} \frac{I_o}{m} \frac{\zeta_T}{a^3} \left\{ \frac{1-e^2}{2} \mathcal{A}_2 + \mathcal{A}_4 + 2e \mathcal{A}_0 \right\} \mathbf{e}_A \\ &\quad + \frac{3c}{2\ell} \frac{I_o}{m} \frac{\zeta_T}{a^3} \left\{ \mathcal{A}_5 - \frac{1-e^2}{2} \mathcal{A}_1 \right\} \mathbf{e}_H + \frac{I_o}{m} \frac{k_o \zeta_c}{6a^4} \mathcal{A}_3 \mathbf{e}_H. \end{aligned} \quad (5.69)$$

Given that $\mathbf{A} = e (\cos \varpi \mathbf{e}_1 + \sin \varpi \mathbf{e}_2) = e \mathbf{e}_A$ and $\dot{\mathbf{e}}_A = \dot{\varpi} \mathbf{e}_H$, we deduce:

$$\dot{\mathbf{A}} = \dot{e} \mathbf{e}_A + \dot{\varpi} e \mathbf{e}_H. \quad (5.70)$$

Thus, the final averaged equations are:

² The gravity field coefficient J_2 (dynamic form factor) is related to $I_o \langle b_{d33} \rangle$ by means of $I_o \langle b_{d33} \rangle = -\frac{2}{3} m R^2 J_2$ that implies

$$J_2 = \frac{I_o}{m R^2} k_o \left(\frac{\zeta_c}{3} + \frac{\zeta_T}{(1-e^2)^{3/2}} \right) \quad (5.66)$$

$$\begin{aligned}
\dot{e} &= \frac{3c}{2\ell} \frac{I_o}{m} \frac{\zeta_T}{a^3} \left\{ \frac{1-e^2}{2} \mathcal{A}_2 + \mathcal{A}_4 + 2e \mathcal{A}_0 \right\} \\
e\dot{\omega} &= \frac{3c}{2\ell} \frac{I_o}{m} \frac{\zeta_T}{a^3} \left\{ \mathcal{A}_5 - \frac{1-e^2}{2} \mathcal{A}_1 \right\} + \frac{I_o}{m} \frac{k_o \zeta_c}{6a^4} \mathcal{A}_3 \\
\dot{\ell} &= 3c \frac{I_o}{m} \frac{\zeta_T}{a^3} \mathcal{A}_0 \\
\dot{\ell}_s &= -3c \frac{I_o}{m} \frac{\zeta_T}{a^3} \mathcal{A}_0 \\
\ell_T &= \ell + \ell_s = \text{constant} \\
\ell_s &= \omega I_o (1 - \langle b_{d33} \rangle) \\
\mathcal{A}_0 &= \sum_{k=-\infty}^{\infty} \left(X_k^{-3,2} \right)^2 \text{Im } k_2(kn - 2\omega) \\
\mathcal{A}_2 &= \sum_k (5X_k^{-4,3} - X_k^{-4,1}) X_k^{-3,2} \text{Im } k_2(kn - 2\omega) + 2X_k^{-4,1} X_k^{-3,0} \text{Im } k_2(nk) \\
\mathcal{A}_4 &= \sum_k X_k^{-3,2} (X_k^{-3,1} + X_k^{-3,3}) \text{Im } k_2(kn - 2\omega) \\
\mathcal{A}_1 &= - \sum_k (X_k^{-4,1} + 5X_k^{-4,3}) X_k^{-3,2} \text{Re } k_2(nk - 2\omega) + 2X_k^{-4,1} X_k^{-3,0} \text{Re } k_2(nk) \\
\mathcal{A}_3 &= X_0^{-4,1} \\
\mathcal{A}_5 &= \sum_k (X_k^{-3,3} - X_k^{-3,1}) X_k^{-3,2} \text{Re } k_2(kn - 2\omega) \\
\langle b_{d33} \rangle &= -\frac{2}{3} k_o \left(\frac{\zeta_c}{3} + \frac{\zeta_T}{(1-e^2)^{3/2}} \right) \\
\zeta_c &= \frac{R^5 \omega^2}{G I_o} \\
\zeta_T &= \frac{m_0 R^5}{2 I_o a^3} \\
\mu &= \frac{m_0 m}{m_0 + m} \\
c &= G m m_0 \\
n^2 a^3 &= G(m_0 + m) \\
\frac{\ell}{\mu a^2} &= n \sqrt{1 - e^2}.
\end{aligned} \tag{5.71}$$

5.1 Computation of Hansen coefficients

The Hansen coefficients depend solely on the eccentricity. Following [Cherniack \(1972\)](#), we express, for $n < 0$ and $m \geq 0$,

$$\left(\frac{r}{a}\right)^n e^{imf} = \left(\sum_{k=-\infty}^{\infty} X_k^{-1,0}(e)e^{ikM}\right)^{|n|} \left(\sum_{l=-\infty}^{\infty} X_l^{0,1}(e)e^{ilM}\right)^m. \quad (5.72)$$

Thus, to compute any series $\left(\frac{r}{a}\right)^n e^{imf}$, one can employ series multiplication of the fundamental series of a/r and e^{if} . This multiplication can be efficiently executed with an algebraic manipulator.

For the computation of the series for $\frac{a}{r}$ and e^{if} , one can refer to [Murray and Dermott \(2000\)](#) Section 2.5:

$$\begin{aligned} \frac{a}{r} &= \frac{e \cos f + 1}{1 - e^2} \\ \cos f &= \frac{e^{if} + e^{-if}}{2} = -e + 2\frac{1 - e^2}{e} \sum_{k=1}^{\infty} J_k(ke) \cos(kM) \\ \sin f &= \frac{e^{if} - e^{-if}}{2i} = 2\sqrt{1 - e^2} \sum_{k=1}^{\infty} \frac{1}{k} \frac{d}{de} J_k(ke) \sin(kM) \\ J_k(x) &= \frac{1}{k!} \left(\frac{x}{2}\right)^k \sum_{l=0}^{\infty} (-1)^l \frac{\left(\frac{x}{2}\right)^{2l}}{l!(k+1)(k+2)\dots(k+l)}, \end{aligned} \quad (5.73)$$

where $J_k(x)$ denotes the Bessel function. The series for $J_k(x)$ converges absolutely for all values of x .

Up to second order in eccentricity and with $e^{iM} = z$ the fundamental series are:

$$\begin{aligned} \frac{r}{a} &= 1 - e\frac{1}{2}(z + z^{-1}) + e^2\left(\frac{1}{2} - \frac{1}{4}(z^2 + z^{-2})\right) + \mathcal{O}(e^3) \\ \frac{a}{r} &= 1 + e\frac{1}{2}(z + z^{-1}) + e^2\frac{(z^2 + z^{-2})}{2} + \mathcal{O}(e^3) \\ e^{if} &= z \left\{ 1 + e(z - z^{-1}) + e^2\left(\frac{9z^2}{8} - 1 - \frac{z^{-2}}{8}\right) \right\} + \mathcal{O}(e^3) \\ e^{-if} &= z^{-1} \left\{ 1 + e(z^{-1} - z) + e^2\left(\frac{9z^{-2}}{8} - 1 - \frac{z^2}{8}\right) \right\} + \mathcal{O}(e^3) \end{aligned} \quad (5.74)$$

These expressions and equation (5.72) imply $X_k^{n,m} = \mathcal{O}(e^{|m-k|})$.

5.2 The equations in [Correia and Valente \(2022\)](#)

Some relations between the Hansen coefficients presented in [Correia and Valente \(2022\)](#), equations (158) and (159), are:

$$\begin{aligned}\sqrt{1-e^2}kX_k^{-3,0} &= \frac{3}{2}e(X_k^{-4,1} - X_k^{-4,-1}) = \frac{3}{2}e(X_k^{-4,1} - X_{-k}^{-4,1}), \\ \sqrt{1-e^2}kX_k^{-3,2} &= \frac{e}{2}(5X_k^{-4,3} - X_k^{-4,1}) + 2X_k^{-4,2}, \\ X_k^{-3,3} &= \frac{1}{e} \left(2(1-e^2)X_k^{-4,2} - 2X_k^{-3,2} - eX_k^{-3,1} \right).\end{aligned}\tag{5.75}$$

One can use these equations to simplify equations (5.71). After such simplifications, the equation governing the eccentricity is:

$$\begin{aligned}\dot{e} &= \frac{3c}{2\ell} \frac{I_o}{m} \frac{\zeta_T}{a^3} \frac{1-e^2}{3e} \sum_{k=-\infty}^{\infty} \left\{ k\sqrt{1-e^2}(X_k^{-3,0})^2 \text{Im } k_2(nk) \right. \\ &\quad \left. - 3 \left(2 - k\sqrt{1-e^2} \right) (X_k^{-3,2})^2 \text{Im } k_2(kn - 2\omega) \right\}.\end{aligned}\tag{5.76}$$

For further simplification, one can apply $\ell = \mu\sqrt{G(m+m_0)a(1-e^2)}$, yielding:

$$\begin{aligned}\dot{e} &= n \frac{m_0}{m} \frac{R^5}{a^5} \frac{\sqrt{1-e^2}}{4e} \sum_{k=-\infty}^{\infty} \left\{ k\sqrt{1-e^2}(X_k^{-3,0})^2 \text{Im } k_2(nk) \right. \\ &\quad \left. - 3 \left(2 - k\sqrt{1-e^2} \right) (X_k^{-3,2})^2 \text{Im } k_2(kn - 2\omega) \right\}.\end{aligned}\tag{5.77}$$

This result corresponds to equation (129) in [Correia and Valente \(2022\)](#).

Our expression for the variation of the longitude of the periapsis, $\dot{\varpi}$, differs from equation (130) in [Correia and Valente \(2022\)](#) due to the neglect of centrifugal deformation in the cited work.

6 Averaged Equations: A Geometrical Approach

In the following two sections, we analyze equation (5.71) from a geometric perspective using singular perturbation theory.

The longitude of the periapsis, ϖ , is absent from the equation for \dot{e} in (5.71). Therefore, the dynamics of the state variables e, ℓ , and ℓ_s can be analyzed independently of ϖ . The conservation of total angular momentum, $\ell_T = \ell + \ell_s$, implies that it is sufficient to observe the dynamics of e and ℓ_s .

While the dynamics unfolds within two-dimensional surfaces, on the level sets of angular momentum, analyzing the equations within a three-dimensional phase space proves more insightful. This approach facilitates a comprehensive

understanding of the global dynamics and the impact of varying angular momentum. After some investigation, we selected (ω, e, a) as the phase-space variables, with $n = \sqrt{\frac{G(m+m_0)}{a^3}}$ being a derived quantity. The differential equation for $a = \frac{\ell^2}{\mu c(1-e^2)}$ is obtained from the equations for $\dot{\ell}$ and \dot{e} . Henceforth we use the approximation

$$\ell_s = \omega I_o(1 - \langle b_{d33} \rangle) \approx \omega I_o.$$

Equations (5.71) and the identity $\frac{3c}{mn^2a^3} = \frac{3m_0}{m+m_0}$ imply

$$\begin{aligned} \frac{\dot{\omega}}{n^2} &= - \left(\frac{3m_0}{m+m_0} \zeta_T \right) \mathcal{A}_0 \\ \frac{\dot{e}}{n} &= \left(\frac{3m_0}{m+m_0} \zeta_T \right) \frac{I_o}{\mu a^2} \frac{1}{2\sqrt{1-e^2}} \left\{ \frac{1-e^2}{2} \mathcal{A}_2 + \mathcal{A}_4 + 2e \mathcal{A}_0 \right\} \\ \frac{\dot{a}}{n} &= \left(\frac{3m_0}{m+m_0} \zeta_T \right) \frac{I_o}{\mu a^2} \frac{a}{(1-e^2)^{3/2}} \left\{ e \left(\frac{1-e^2}{2} \mathcal{A}_2 + \mathcal{A}_4 \right) + 2 \mathcal{A}_0 \right\}. \end{aligned} \quad (6.78)$$

Conservation of angular momentum $\ell_T = \sqrt{\mu c a} \sqrt{1-e^2} + I_o \omega$ implies

$$\frac{\omega}{n} = \frac{\ell_T}{I_o n} \left(1 - \sqrt{\frac{a \mu c}{\ell_T^2}} \sqrt{1-e^2} \right). \quad (6.79)$$

This suggests the following nondimensionalization of a :

$$\tilde{a} := \frac{a}{a_o}, \quad \text{where} \quad a_o := \frac{\ell_T^2}{\mu c} \quad (6.80)$$

is defined as the radius of the circular orbit for two point masses, m_0 and m , possessing an orbital angular momentum of $\ell = \ell_T$.

Let

$$n_o = \frac{\ell_T}{\mu a_o^2} = \frac{c^2 \mu}{\ell_T^3} \quad (6.81)$$

be the angular frequency of the circular orbit of radius a_o . Kepler's third law implies, $n^2 a^3 = G(m+m_0) = n_o^2 a_o^3$ and so

$$n = n_o \frac{1}{\tilde{a}^{3/2}}. \quad (6.82)$$

Conservation of angular momentum, as expressed in equation (6.79), implies

$$\frac{\omega}{n} = \epsilon^{-1} \tilde{a}^{\frac{3}{2}} (1 - \tilde{a}^{\frac{1}{2}} \sqrt{1-e^2}), \quad (6.83)$$

where

$$\epsilon := \frac{I_o}{\mu a_o^2} = \frac{I_o n_o}{\ell_T} = \frac{I_o \mu c^2}{\ell_T^4}. \quad (6.84)$$

For the Mercury-Sun system, where m_0 is the mass of the Sun, $\epsilon = 6.8 \times 10^{-10}$, and for the Earth-Moon system, where m_0 is the mass of the Moon, $\epsilon = 0.0036$. Although ϵ appears to be very small for all problems of interest, in this section,

we will conduct a geometric analysis with an arbitrary value of ϵ to elucidate the global properties of the equations.

Using the above definitions equations (6.78) can be written in nondimensional form as

$$\begin{aligned}
\frac{\dot{\omega}}{n_o^2} &= -N \frac{1}{\tilde{a}^6} \mathcal{A}_0 \\
\frac{\dot{e}}{n_o} &= \epsilon N \frac{1}{2\tilde{a}^{13/2} \sqrt{1-e^2}} \left\{ \frac{1-e^2}{2} \mathcal{A}_2 + \mathcal{A}_4 + 2e \mathcal{A}_0 \right\} \\
\frac{\dot{a}}{n_o} &= \epsilon N \frac{1}{\tilde{a}^{11/2} (1-e^2)^{3/2}} \left\{ e \left(\frac{1-e^2}{2} \mathcal{A}_2 + \mathcal{A}_4 \right) + 2 \mathcal{A}_0 \right\} \\
N &= \frac{3m_0}{m+m_0} \zeta_{T_o} \quad \text{where} \quad \zeta_{T_o} = \frac{m_0 R^5}{2 I_o a_o^3} \\
\tilde{a} &= \frac{a}{a_o} \quad \text{where} \quad a_o = \frac{\ell_T^2}{\mu c} \\
n &= n_o \frac{1}{\tilde{a}^{3/2}} \quad \text{where} \quad n_o = \frac{\ell_T}{\mu a_o^2} \\
\epsilon &= \frac{I_o}{\mu a_o^2} = \frac{I_o n_o}{\ell_T} = \frac{I_o \mu c^2}{\ell_T^4},
\end{aligned} \tag{6.85}$$

where μ , c , \mathcal{A}_0 , \mathcal{A}_2 , and \mathcal{A}_4 are given in equation (5.71).

6.1 Estimate of the Rate of Spin Variations.

In a time scale where the unit of time corresponds to one radian of orbital motion, the spin angular velocity is ω/n , and, from equation (6.78), the rate of change of spin is

$$\frac{\dot{\omega}}{n^2} = - \left(\frac{3m_0}{m+m_0} \zeta_T \right) \mathcal{A}_0,$$

where

$$\mathcal{A}_0 = \sum_{k=-\infty}^{\infty} \left(X_k^{-3,2}(e) \right)^2 \text{Im} k_2(kn - 2\omega).$$

From equation (2.13)

$$\text{Im} k_2(kn - 2\omega) = -k_o \frac{\tau(kn - 2\omega)}{1 + \tau^2(kn - 2\omega)^2}, \tag{6.86}$$

and we can express

$$\begin{aligned}
\frac{\dot{\omega}}{n^2} &= V\left(\tau n, \frac{\omega}{n}, e\right) \\
&:= \frac{3m_0}{(m+m_0)} \zeta_T k_o \sum_{k=-\infty}^{\infty} \left(X_k^{-3,2}(e) \right)^2 \frac{\tau n (k - 2\frac{\omega}{n})}{1 + \tau^2 n^2 (k - 2\frac{\omega}{n})^2}.
\end{aligned} \tag{6.87}$$

For a fixed pair (e, n) , $\frac{\dot{\omega}}{n^2} = V(\tau n, \frac{\omega}{n}, e)$ defines a differential equation for $\frac{\omega}{n}$. We aim to estimate two typical quantities associated with V : its maximum and the time constant near a stable equilibrium, as depicted in Figure 2.

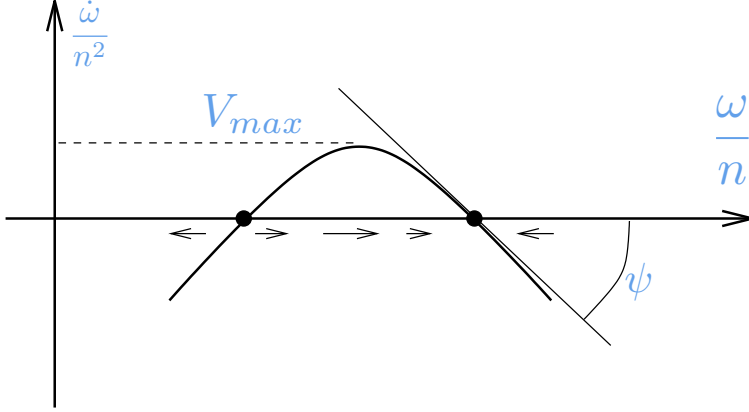


Fig. 2 Vector field $\frac{\dot{\omega}}{n^2} = V(\tau n, \frac{\omega}{n}, e)$ with constant n and e . V_{max} represents the maximum rate of variation of $\frac{\omega}{n}$ and $\tau_s^{-1} = \tan \psi$ denotes the time constant of a stable equilibrium.

The maximum value of the function $\sigma \rightarrow \frac{|\sigma|}{1+\sigma^2}$ is $\frac{1}{2}$. Hence,

$$\sum_{k=-\infty}^{\infty} \left(X_k^{-3,2}(e) \right)^2 \frac{\tau(kn - 2\omega)}{1 + \tau^2(kn - 2\omega)^2} \leq \frac{1}{2} \sum_{k=-\infty}^{\infty} \left(X_k^{-3,2}(e) \right)^2. \quad (6.88)$$

Applying Parseval's identity, we get

$$\sum_{k=-\infty}^{\infty} \left(X_k^{-3,2}(e) \right)^2 = \frac{1}{2\pi} \int_0^{2\pi} \frac{e^{i2f}}{r^3} \frac{e^{-i2f}}{r^3} dM = \frac{1}{2\pi} \int_0^{2\pi} \frac{1}{r^6} dM = X_0^{-6,0}. \quad (6.89)$$

Based on [Laskar and Boué \(2010\)](#), $X_0^{-6,0} = \frac{3e^4 + 3e^2 + 1}{(1-e^2)^{9/2}}$ leading to

$$\sum_{k=-\infty}^{\infty} \left(X_k^{-3,2}(e) \right)^2 \frac{\tau(kn - 2\omega)}{1 + \tau^2(kn - 2\omega)^2} \leq \frac{1}{2} \frac{3e^4 + 3e^2 + 1}{(1 - e^2)^{9/2}}. \quad (6.90)$$

The right side of this inequality increases with e , with values: $1/2$ for $e = 0$, approximately 1.6 for $e = 0.4$, approximately 3.3 for $e = 0.5$, and approximately 8 for $e = 0.6$. Since $\frac{m_0}{m+m_0} \leq 1$, we deduce

$$\frac{\dot{\omega}}{n^2} \leq 10 \zeta_\tau k_0 \quad \text{when } e < 0.5. \quad (6.91)$$

It is worth noting that ζ_τ , defined in equation (3.21), is a small quantity.

For sufficiently large values of τn , the stable equilibria of $\frac{\omega}{n}$ are close to semi-integers $\frac{k}{2}$, with $k = 1, 2, \dots$, and for these values, the dominant term in the sum of V is the k^{th} -term [Correia et al. \(2014\)](#). Thus, equation (6.87) yields the time constant

$$\tau_k^{-1} \approx \frac{3m_0}{(m + m_0)} \zeta_T k_o \left(X_k^{-3,2}(e) \right)^2 \tau n, \quad (6.92)$$

for an equilibrium $\frac{\omega}{n} \approx \frac{k}{2}$.

Note that V_{max} is independent of the characteristic time of the rheology τ , whereas the time constant τ_k has a linear dependency. A maximum rate speed V_{max} proportional to $\zeta_T k_o$ will be observed during spin jumps. The prefactor 10 in equation (6.91) varies with the eccentricity e .

6.2 Equilibria, Linearization and the Invariant Subspace of Zero Eccentricity.

Using the expressions for the Hansen coefficients in Section 5.1 we can compute the expansion of the right-hand side of equation (6.85) up to first order in eccentricity:

$$\begin{aligned} \frac{\dot{\omega}}{n_o^2} &= k_o \frac{N}{\tilde{a}^6} \frac{\tau(2n - 2\omega)}{\tau^2(2n - 2\omega)^2 + 1} \\ \frac{\dot{\tilde{a}}}{n_o} &= -k_o \frac{\epsilon N}{\tilde{a}^{11/2}} \frac{2\tau(2n - 2\omega)}{\tau^2(2n - 2\omega)^2 + 1} \\ \frac{\dot{e}}{n_o} &= -k_o \frac{\epsilon N}{2\tilde{a}^{13/2}} \frac{1}{4} e \tau n \left(\frac{6}{n^2 \tau^2 + 1} + \frac{8\frac{\omega}{n} - 8}{4\tau^2 n^2 (1 - \frac{\omega}{n})^2 + 1} \right. \\ &\quad \left. + \frac{2\frac{\omega}{n} - 1}{\tau^2 n^2 (1 - 2\frac{\omega}{n})^2 + 1} + \frac{49(3 - 2\frac{\omega}{n})}{\tau^2 n^2 (3 - 2\frac{\omega}{n})^2 + 1} \right) \\ n &= n_o \frac{1}{\tilde{a}^{3/2}} \end{aligned} \quad (6.93)$$

These equations imply that the plane $e = 0$ is invariant.

The only equilibria of equations (6.85) are on the plane $e = 0$, as shown in the next paragraph, and are given by the curve

$$\frac{\omega}{n} = 1. \quad (6.94)$$

The equilibria of (6.85) satisfy $\mathcal{A}_0 = 0$ and $\frac{1-e^2}{2}\mathcal{A}_2 + \mathcal{A}_4 = 0$. Equation (5.76) shows that these equations imply

$$\begin{aligned} &n \sum_{k=-\infty}^{\infty} \left\{ k(X_k^{-3,0})^2 \text{Im } k_2(nk) + 3k(X_k^{-3,2})^2 \text{Im } k_2(kn - 2\omega) \right\} \\ &= \sum_{k=-\infty}^{\infty} \left\{ (X_k^{-3,0})^2 (nk) \text{Im } k_2(nk) + 3(X_k^{-3,2})^2 (kn - 2\omega) \text{Im } k_2(kn - 2\omega) \right\} = 0. \end{aligned} \quad (6.95)$$

We notice, from (6.86), that $x\text{Im } k_2(x) < 0 \forall x \neq 0$ and hence (6.95) holds if and only each term of the sum is zero. The Hansen coefficients have the following properties: $\forall k \neq 0, X_k^{-3,0}(e) = 0 \iff e = 0$ and $\forall k \neq 2, X_k^{-3,2}(e) = 0 \iff e = 0$. This implies that $e = 0$ is a necessary condition for the existence of an equilibrium.

Conservation of angular momentum implies that the orbits of the vector field (6.93) in the plane where $e = 0$ are parameterized by angular momentum. Equation (6.83) shows that the representation of these orbits in the plane $(\tilde{a}, \frac{\omega}{n})$ is given by the graphs

$$\tilde{a} \mapsto \epsilon^{-1} \tilde{a}^{\frac{3}{2}} (1 - \tilde{a}^{\frac{1}{2}}) = \frac{\omega}{n}, \quad \text{for } \epsilon \in (0, \infty), \quad (6.96)$$

as illustrated in Figure 3.

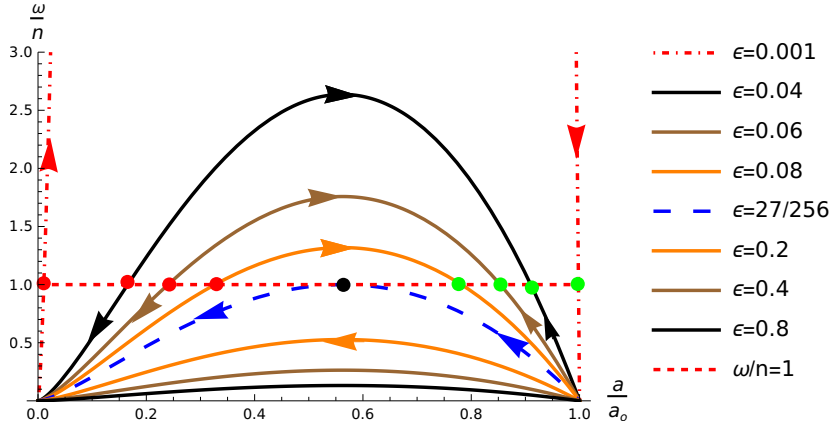


Fig. 3 Orbits of the equation (6.85) on the invariant plane $e = 0$. The orbits are labelled by the total angular momentum ℓ_T by means of the nondimensional parameter $\epsilon^{-1} = \frac{\ell_T^4}{I_o \mu c^2}$. The equilibria are on the horizontal line $\frac{\omega}{n} = 1$: the green dots represent stable equilibria and the red dots represent unstable equilibria. The black dot at $\tilde{a} = \frac{9}{16}, \frac{\omega}{n} = 1$ represents the single equilibrium that occurs for the special value $\epsilon = \frac{27}{256}$. For $\epsilon > \frac{27}{256}$ (small angular momentum) all the solutions lead to a collision.

In the significant case where $\epsilon \approx 0$, equation (6.83) suggests that $0 \approx \epsilon \frac{\omega}{n} = \tilde{a}^{\frac{3}{2}} (1 - \tilde{a}^{\frac{1}{2}} \sqrt{1 - e^2})$. Up to first order in eccentricity, we have $\tilde{a} = 1$ and $n = n_o$. Using this approximation, the function $\frac{\dot{e}}{e}$ in equation (6.93) is expressed as

$$\frac{\dot{e}}{e} = -\tilde{c} \left(\frac{6}{n^2 \tau^2 + 1} + \frac{8 \frac{\omega}{n} - 8}{4 \tau^2 n^2 (1 - \frac{\omega}{n})^2 + 1} + \frac{2 \frac{\omega}{n} - 1}{\tau^2 n^2 (1 - 2 \frac{\omega}{n})^2 + 1} + \frac{49(3 - 2 \frac{\omega}{n})}{\tau^2 n^2 (3 - 2 \frac{\omega}{n})^2 + 1} \right), \quad (6.97)$$

where $n = n_o = \text{constant}$ and \tilde{c} is a positive, although small, constant. The graph of $\frac{\dot{e}}{e\tilde{c}}$ as a function of $\frac{\omega}{n}$ for various values of τn is depicted in Figure 4.

This figure illustrates that $\frac{\dot{e}}{e\dot{c}}$ changes sign near the plane $e = 0$. Consequently, a solution with an initial eccentricity close to zero, yet sufficiently distant from the stable equilibrium at $\frac{\omega}{n} = 1$, may experience an increase in eccentricity.

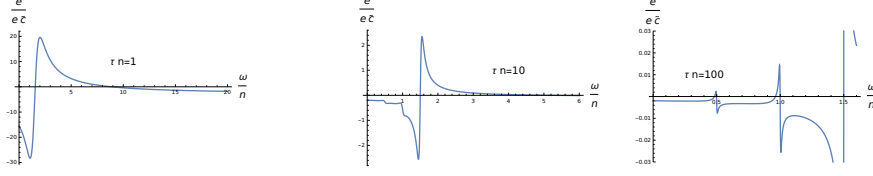


Fig. 4 The graph of $\frac{\dot{e}}{e\dot{c}}$ as a function of $\frac{\omega}{n}$ for values of τn equal 1, 10, and 100. For $n = 10$, $\frac{\dot{e}}{e\dot{c}}$ has a zero, not easily seen in the Figure, at $\frac{\omega}{n} = 5.26$.

The next step in understanding the dynamics of equation (6.85) involves linearization about the equilibria. It is evident from Figure 3 that the equilibria can be parameterized by their \tilde{a} coordinate. Thus, an equilibrium is represented by $(\omega, \tilde{a}) = (\omega_e, \tilde{a}_e)$, where, according to equation (6.83), \tilde{a}_e is the solution to

$$\epsilon = \tilde{a}^{\frac{3}{2}}(1 - \tilde{a}^{\frac{1}{2}}). \quad (6.98)$$

The special equilibrium $\tilde{a}_e = \frac{9}{16}$, corresponding to the bifurcation value $\epsilon = \frac{27}{256}$, marked by the black dot in Figure 3, represents a threshold of stability: an equilibrium with $\tilde{a}_e < \frac{9}{16}$ is unstable, while an equilibrium with $\tilde{a}_e > \frac{9}{16}$ is stable.

Given that $0 < \epsilon < \frac{27}{256} \approx 0.1$, a perturbative calculation reveals that the largest root of this equation (stable equilibrium) satisfies

$$\tilde{a}_e = 1 - 2\epsilon - 5\epsilon^2 + \mathcal{O}(\epsilon^3). \quad (6.99)$$

This approximation remains accurate up to $\epsilon = 0.05$.

At equilibrium, the orbit is circular. If $\ell_e = \ell_T - I_o n_e$ denotes the orbital angular momentum at equilibrium, then $a_e = \frac{\ell_e^2}{\mu c}$. Since $a_e = \tilde{a}_e a_o$ and $a_o = \frac{\ell_T^2}{\mu c}$, we obtain

$$\tilde{a}_e = \left(\frac{\ell_e}{\ell_T}\right)^2 = \left(1 - \frac{I_o n_e}{\ell_T}\right)^2. \quad (6.100)$$

Thus, \tilde{a}_e represents the square of the ratio of orbital angular momentum to total angular momentum at equilibrium. For the Mercury-Sun system, where m_o is the mass of the Sun, $\epsilon = 6.8 \times 10^{-10}$ and $\tilde{a}_e \approx 1$. For the Earth-Moon system, where m_o is the mass of the Moon, $\epsilon = 0.0036$ and $\tilde{a}_e = 0.993$. It appears that in most problems of interest, $\tilde{a}_e \approx 1$.

The linearization of equation (6.85) at $(\omega, \tilde{a}, e) = (\omega_e, \tilde{a}_e, 0)$ is derived easily from equation (6.93):

$$\begin{aligned}\dot{\delta}_\omega &= -k_o \frac{N\tilde{n}_e^2\tau}{\tilde{a}_e^3} \left(2\delta_\omega + 3\frac{\tilde{n}_e}{\tilde{a}_e}\delta_a \right) = \left(\frac{k_o N\tilde{n}_e\tau}{\tilde{a}_e^3} \right) \tilde{n}_e \left(-2\delta_\omega - 3\frac{\tilde{n}_e}{\tilde{a}_e}\delta_a \right), \\ \dot{\delta}_a &= k_o \frac{2N\tilde{n}_e\epsilon\tau}{\tilde{a}_e^4} \left(2\delta_\omega + 3\frac{\tilde{n}_e}{\tilde{a}_e}\delta_a \right) = \left(\frac{k_o N\tilde{n}_e\tau}{\tilde{a}_e^3} \right) \frac{2\epsilon}{\tilde{a}_e} \left(2\delta_\omega + 3\frac{\tilde{n}_e}{\tilde{a}_e}\delta_a \right), \\ \dot{e} &= -k_o \frac{N\tilde{n}_e^2\epsilon\tau}{\tilde{a}_e^5} \frac{7}{1 + \tilde{n}_e^2\tau^2} e = - \left(\frac{k_o N\tilde{n}_e\tau}{\tilde{a}_e^3} \right) \frac{\tilde{n}_e\epsilon}{\tilde{a}_e^2} \frac{7}{1 + \tilde{n}_e^2\tau^2} e,\end{aligned}\tag{6.101}$$

where $\tilde{n}_e = n_0 \frac{1}{\tilde{a}_e^{3/2}}$. Each equilibrium has: one eigenvalue equal to zero, associated with the conservation of angular momentum; one negative eigenvalue $\lambda_e = -\frac{7\tilde{n}_e\epsilon}{\tilde{a}_e^2(\tilde{n}_e^2\tau^2+1)} \left(\frac{k_o N\tilde{n}_e\tau}{\tilde{a}_e^3} \right)$, with an eigenvector tangent to the eccentricity axis; and one eigenvalue $\lambda_0 = -\frac{2\tilde{n}_e(\tilde{a}_e^2-3\epsilon)}{\tilde{a}_e^2} \left(\frac{k_o N\tilde{n}_e\tau}{\tilde{a}_e^3} \right)$, with an eigenvector in the plane $e = 0$ and tangent to the surface of constant angular momentum. As expected, $\lambda_0 = 0$ in the critical case where $\epsilon = \frac{27}{256}$ and $\tilde{a}_e = \frac{9}{16}$, $\lambda_0 > 0$ if $\tilde{a}_e < \frac{9}{16}$, and $\lambda_0 < 0$ if $\tilde{a}_e > \frac{9}{16}$.

Consider a solution to equation (6.93) that satisfies $\lim_{t \rightarrow \infty} (e(t), \tilde{a}(t)) = (0, \tilde{a}_e)$, and let $\delta_a(t) = \tilde{a}(t) - \tilde{a}_e$. At a certain time \tilde{t} , this solution is sufficiently close to $(0, \tilde{a}_e)$ for the linear approximation to be valid. Since $\delta_a(t) = e^{\lambda_0(t-\tilde{t})}\delta_a(\tilde{t})$ and $e(t) = e^{\lambda_e(t-\tilde{t})}e(\tilde{t})$, we conclude that near the equilibrium,

$$\delta_a(e) = \tilde{a}(e) - \tilde{a}_e = \underbrace{\frac{\delta_a(\tilde{t})}{e^{\lambda_0/\lambda_e}(\tilde{t})}}_{=\text{constant}} e^{\lambda_0/\lambda_e}, \tag{6.102}$$

where

$$\frac{\lambda_0}{\lambda_e} = \frac{2(\tilde{a}_e^2 - 3\epsilon)}{7\epsilon} (\tilde{n}_e^2\tau^2 + 1) = \frac{8(\sqrt{\tilde{a}_e} - \frac{3}{4})}{7(1 - \sqrt{\tilde{a}_e})} (\tilde{n}_e^2\tau^2 + 1). \tag{6.103}$$

Regardless of the value of the constant factor in equation (6.102), which in Figure 5 we assume to be one, the orbit's geometry near the equilibrium is controlled by the ratio $\frac{\lambda_0}{\lambda_e}$. In Figure 5 LEFT, we illustrate how the orbit changes as $\frac{\lambda_0}{\lambda_e}$ varies, with the ratio $\frac{\lambda_0}{\lambda_e} = 1$ being a critical value. For $\frac{\lambda_0}{\lambda_e} > 1$, the orbit approaches the equilibrium along the e -axis, and for $0 < \frac{\lambda_0}{\lambda_e} < 1$, the orbit approaches the equilibrium along the δ_a axis. In Figure 5 RIGHT, we demonstrate how to determine the special value of \tilde{a}_e , corresponding to $\frac{\lambda_0}{\lambda_e} = 1$, as a function of the parameter $\tau\tilde{n}_e$. The maximal value of this special \tilde{a}_e is $\frac{169}{225} \approx 0.75$, achieved when $\tau = 0$.

It appears that in most problems of interest, ϵ is very small, $\tilde{a}_e \approx 1$, and $\lambda_0/\lambda_e \gg 1$, indicating that solutions approach the stable equilibrium along the e -axis, namely the weak-stable manifold of the equilibrium.

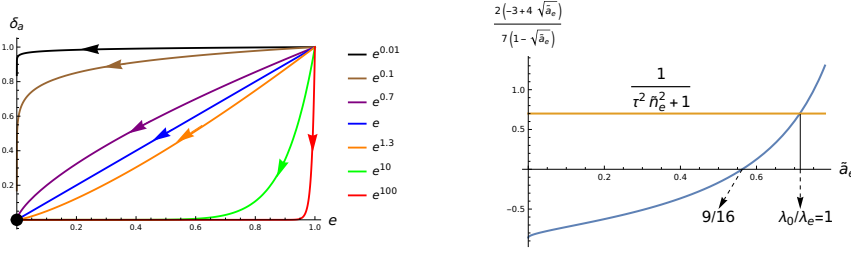


Fig. 5 LEFT: The figure shows possible orbits on the eccentricity-semi-major axis ($\delta_a = \tilde{a} - \tilde{a}_e$) plane, $\delta_a = \text{constant } e^{\lambda_0/\lambda_e}$ with constant = 1 for various λ_0/λ_e values. RIGHT: A graphical method to find the special value of \tilde{a}_e , where $\lambda_0/\lambda_e = 1$, as a function of $\tau \tilde{n}_e$.

6.3 Slow-fast systems and singular perturbation theory

For $\epsilon \approx 0$ equation (6.93) has the form of a slow-fast system:

$$\begin{aligned} \dot{x} &= f(x, y, \epsilon), \\ \dot{y} &= \epsilon g(x, y, \epsilon), \end{aligned} \quad (6.104)$$

with $x = \omega \in \mathbb{R}$ as the fast variable and $y = (e, \tilde{a}) \in \mathbb{R}^2$ as the slow variables Fenichel (1979).

Given an initial condition in the state space $\{\omega, e, \tilde{a}\}$, the value of ω varies while (e, \tilde{a}) stays nearly constant until the state reaches the slow manifold

$$\Sigma_s(0) := \{\dot{\omega}(\omega, e, \tilde{a}) = 0\} = \{\mathcal{A}_0(\omega, e, \tilde{a}) = 0\} \quad (\text{s denotes slow}), \quad (6.105)$$

where \mathcal{A}_0 is given in equation (5.71).

When (x, y_0) is not close to $\Sigma_s(0)$, the fast dynamics is governed by the layer problem, $\dot{x} = f(x, y_0, 0)$. Here, the fast dynamics corresponds to the fast spin variation with fixed e and \tilde{a} . The spin decreases on points above $\Sigma_s(0)$ and increases on points under $\Sigma_s(0)$, see Figure 10. Close to the slow manifold $\Sigma_s(0)$, the dynamics is approximated by the reduced problem, where the fast variable is given by an implicit function, solution of $f(\Phi(y), y, 0) = 0$, and the slow variable solves the differential equation on $\Sigma_s(0)$, $\dot{y} = g(\Phi(y), y, 0)$. The implicit function theorem ensures that Φ is locally determined at $(x_0, y_0) \in \Sigma_s$ if $\partial_x f(x_0, y_0, 0) \neq 0$. In this case, $\Sigma_s(0)$ is called normally hyperbolic at (x_0, y_0) . The results from geometric singular perturbation theory Fenichel (1979) state that if the system (6.104) has a normally hyperbolic slow manifold S_0 , for each small $\epsilon > 0$ exists an invariant manifold S_ϵ diffeomorphic to S_0 which is stable (unstable) if $\partial_x f < 0$ ($\partial_x f > 0$) on S_0 . We will denote by $\Sigma_s(\epsilon)$ the union of the hyperbolic components of perturbed slow manifold in (6.105).

The dynamics across the entire phase space can be elucidated by examining the geometry of the slow manifold (6.105). Within the first octant $\mathcal{B}_1 := \{\omega > 0, e > 0, a > 0\}$, $\Sigma_s(0)$ possesses a single connected component that splits \mathcal{B}_1 into two regions. The conservation of angular momentum reduces the analysis to a two-dimensional problem. A diagram illustrating the local behavior of orbits near the stable equilibrium is presented in Figure 5 LEFT. A global

illustration of the flow on a level set of angular momentum is shown in Figure 6.

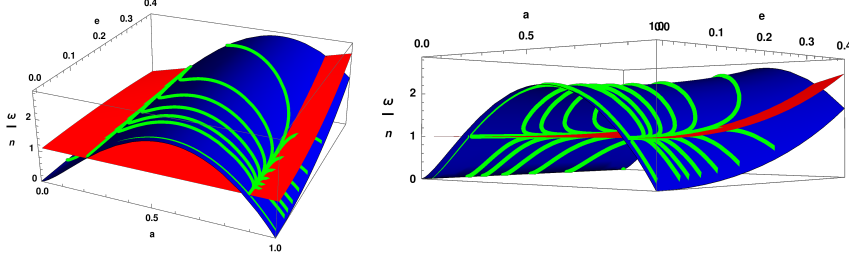


Fig. 6 The phase space close to the synchronous states $\omega/n = 1$, $e = 0$. The blue surface represents a level set of the angular momentum and the red surface represents the slow manifold $\Sigma_s(\epsilon)$. Both surfaces and the plane $e = 0$ intersect only at the equilibria. The stable separatrix of the saddle point delimits the basin of attraction of the node and the region whose solutions tend to the collision $a = 0$.

7 Spin-Orbit Resonances

In this section, we assume that the ratio $\frac{\omega}{n}$ is at most on the order of tens, so that

$$\left| \epsilon \frac{\omega}{n} \right| \ll 1. \quad (7.106)$$

Under this condition, equation (6.83), i.e., $\tilde{a}^{\frac{3}{2}}(1 - \tilde{a}^{\frac{1}{2}}\sqrt{1 - e^2}) = \epsilon \frac{\omega}{n}$, yields two solutions for \tilde{a} . The first solution is $\tilde{a} = (\epsilon \frac{\omega}{n})^{2/3} + \mathcal{O}(\epsilon)$. This solution closely approximates the surface of constant angular momentum in a region that includes the unstable equilibrium $\tilde{a}_e \approx 0$. This approximation is depicted in Figure 3 by the nearly vertical red dot-dashed line near $\tilde{a}_e \approx 0$. We will not focus on this region. The second solution is $\tilde{a} = \frac{1}{1 - e^2} + \mathcal{O}(\epsilon)$, which is of primary interest. This solution approximates the surface of constant angular momentum in a region containing the stable equilibrium $\tilde{a}_e \approx 1$. This approximation is depicted in Figure 3 by the nearly vertical red dot-dashed line near $\tilde{a}_e \approx 1$. Disregarding the error of order ϵ , we have $\tilde{a}_e = 1$, $a_e = a_o$, and

$$\tilde{a} = \frac{1}{1 - e^2} \Rightarrow a = a_o \frac{1}{1 - e^2}, \quad \text{where} \quad a_o = \frac{\ell^2}{\mu c}. \quad (7.107)$$

In the subsequent analysis we use these approximations.

The geometry of the slow manifold $\Sigma_s(0)$ plays a crucial role in the capture into spin-orbit resonance, particularly where $\Sigma_s(0)$ is not normally hyperbolic. The slow manifold becomes non-normally hyperbolic at points where the projection map from $\Sigma_s(0)$ to the $\{a, e\}$ plane is singular. These generic singular

points of the projection are known as folds and collectively form the “fold curves”. In Figure 7, the fold curves are depicted in blue on the slow manifold $\Sigma_s(0)$, which is represented as an orange surface. Although the fold curves themselves are smooth, their projection onto the $\{a, e\}$ plane includes singular points termed “cusps”, at which a moving point on the projection reverses direction. A cusp point on a fold curve occurs where the tangent to the curve becomes parallel to the ω -axis. The flow dynamics near a fold are extensively described in the literature [Krupa and Szmolyan \(2001a\)](#).

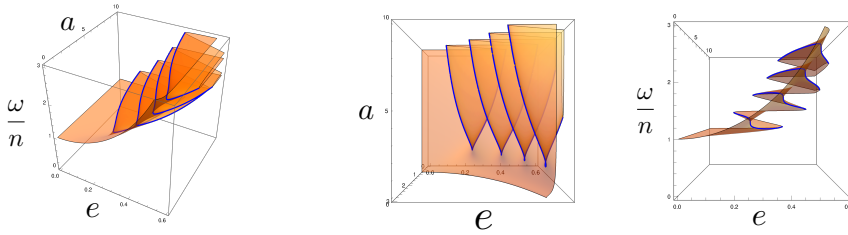


Fig. 7 Figure showing three views of the slow manifold $\Sigma_s(0)$, which is the orange surface, and the fold curves in blue.

We illustrate the so called phenomenon of capture into spin-orbit resonance by a concrete example presented in [Correia et al. \(2014\)](#) and [Correia et al. \(2018\)](#). We use the parameters of the exoplanet HD80606b and its hosting star, namely $m_0 = 2008.9 \cdot 10^{30}\text{kg}$, $m = 7.746 \cdot 10^{28}\text{kg}$, $I_o = 8.1527 \cdot 10^{40}\text{kg m}^2$. The initial conditions are chosen as $a = 0.455\text{au}$, $e = 0.9330$ and $\omega = 4\pi\text{ rad/day}$ and hence $\epsilon = 1.35 \cdot 10^{-8}$. The parameters of the rheology are $k_o = 0.5$ and $\tau = 10^{-2}\text{year}$.

In Figures 8 (top panels), the red curve represents a trajectory of the fundamental equations, given in Section 2, which was obtained by means of numerical integration. The numerically computed trajectory has consecutive transitions between stable branches of the perturbed slow manifold $\Sigma_s(\epsilon)$. This trajectory shows a slow decrease of the eccentricity towards $e = 0$ while the spin-orbit ratio has fast transitions between integers and half-integers with final value $\omega/n = 1$. The stable branches of $\Sigma_s(\epsilon)$ are quite flat (parallel to the (e, a) -plane) near the planes $\frac{\omega}{n} = \frac{k}{2}$, $k \in \mathbb{Z}$. These results are detailed in Figure 14 from [Correia et al. \(2018\)](#). We can observe in Figure 8 the full agreement between the solution of the fundamental equations and the fast-slow-geometric analysis of the averaged equations.

The projection of the fold curves to the plane (a, e) are shown in Figure 8 DOWN-RIGHT. Each curve contains a cusp singularity and is labeled by an integer or half-integer. A point initially over (a, e) can be attracted to a resonance $\frac{\omega}{n} = \frac{k}{2}$ only if it is inside a dashed curve that intersects the curve labeled by $\frac{k}{2}$; see caption of Figure 8 for further information.

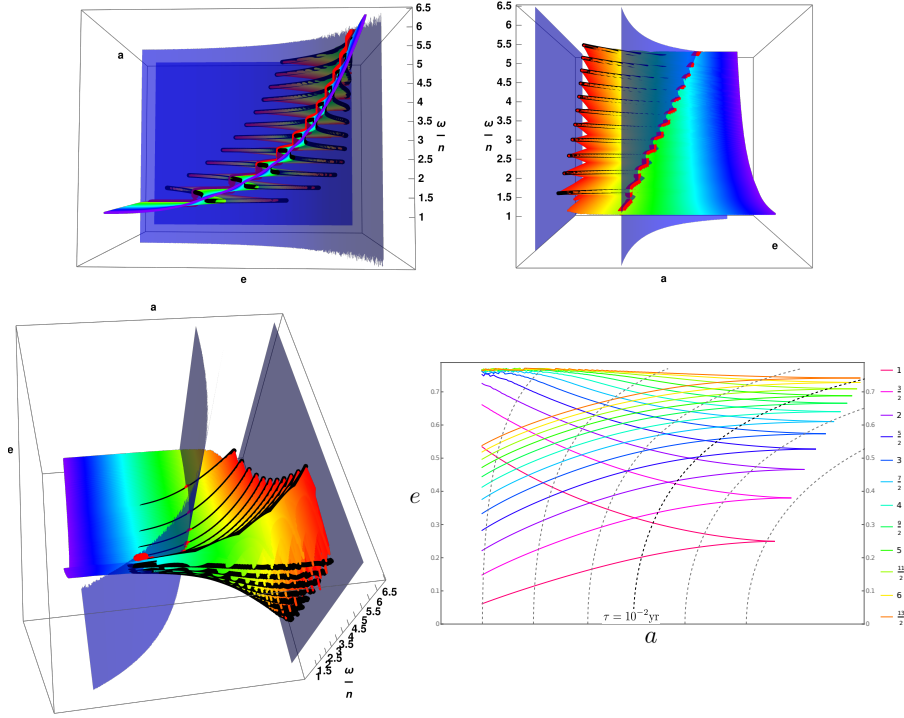


Fig. 8 Geometrical perspective of capture into spin-orbit resonances. The slow manifold $\Sigma_s(0)$ loses normal hyperbolicity at fold curves (black), characterized by $\partial_{\omega}\mathcal{A}_0 = 0$. The fold curves become parallel to the $\frac{\omega}{n}$ -axis at the cusp points. The blue surface represents a level set of angular momentum, as depicted in Figure 6. The red curve represents a solution of the complete system, which exhibits jumps when crossing the fold curves. In the lower-right frame, the projection of the cusp-shaped curves onto the (a, e) plane is displayed. Each curve is annotated with an integer or half-integer, symbolizing a resonance $\omega/n = \frac{k}{2}$, for $k = 1, \dots, 13$, as noted on the right side of the figure. The dashed lines correspond to projections of the constant angular momentum surfaces $a = \frac{\ell_T^2}{\mu c} \frac{1}{1-e^2}$. If the total angular momentum ℓ_T is sufficiently large such that the curve $a = \frac{\ell_T^2}{\mu c} \frac{1}{1-e^2}$ does not intersect the projection of the fold curve associated with a specific $\omega/n = \frac{k}{2}$ spin-orbit resonance, then the $k : 2$ resonance is precluded for that angular momentum value.

7.1 Spin-Orbit Resonances Requires Large Relaxation Times τ .

The approximation $\tilde{a} = (1-e^2)^{-1}$ and equation (6.82) imply $n = n_o(1-e^2)^{3/2}$. The imaginary part of the Love number (6.86) can then be written as

$$\begin{aligned} \text{Im}k_2(kn - 2\omega) &= k_o \frac{2\tau n(\omega/n - k/2)}{1 + (2\tau n)^2(\omega/n - k/2)^2} \\ &= \sqrt{\tilde{\epsilon}}k_o(1-e^2)^{\frac{3}{2}} \frac{(\omega/n - k/2)}{\tilde{\epsilon} + (1-e^2)^3(\omega/n - k/2)^2}, \end{aligned} \quad (7.108)$$

where

$$\tilde{\epsilon} := \frac{1}{(2\tau n_o)^2}, \quad n_o = \frac{c^2 \mu}{\ell_T^3}. \quad (7.109)$$

For $e = 0$, the slow manifold lacks any fold points for any value of $\tau > 0$, as illustrated in Figure 3. Consider a fixed value $e_1 > 0$ for e . Equations (6.87) and (7.108) imply the existence of at least $j - 1$ fold points in the region $\{0 < e < e_1, 0 < \frac{\omega}{n} < C\}$, where $C > 0$ represents a positive constant, if and only if

$$\begin{aligned} \frac{\omega}{n} \mapsto & \left(X_2^{-3,2}(e_1) \right)^2 \frac{(\omega/n - 1)}{\tilde{\epsilon} + (1 - e_1^2)^3 (\omega/n - 1)^2} \\ & + \sum_{k \neq 2} \left(X_k^{-3,2}(e_1) \right)^2 \frac{(\omega/n - k/2)}{\tilde{\epsilon} + (1 - e_1^2)^3 (\omega/n - k/2)^2} \end{aligned} \quad (7.110)$$

has j zeroes for $\frac{\omega}{n} \in (0, C)$.

Given that $X_k^{-3,2}(0) = 1$ and $X_k^{-3,2}(e_1) = \mathcal{O}(e_1)$, function (7.110) can be expressed as $\frac{(\omega/n-1)}{\tilde{\epsilon}+(\omega/n-1)^2} + \mathcal{O}(e_1^2)$. For $0 < \frac{\omega}{n} < C$ and a fixed $\tilde{\epsilon} > 0$, this function exhibits a single zero near $\frac{\omega}{n} = 1$ if $e_1 > 0$ is sufficiently small. Furthermore, for a fixed $e_1 > 0$ and $\tilde{\epsilon} = 0$, function (7.110) presents poles for every $\frac{\omega}{n} = \frac{k}{2}$, $k \in \mathbb{Z}$, thereby ensuring at least one zero in each interval $(k, k + \frac{1}{2})$, where k is any half-integer. A continuity argument suggests that if $\tilde{\epsilon}$ is sufficiently close to zero (implying τ is sufficiently large), then for any fixed e_1 , function (7.110) will have zeroes near $j/2$, for $j = 1, 2, \dots$. This analysis indicates that, particularly for small $e_1 > 0$, the condition $\tilde{\epsilon} \ll 1$ (equivalently, $\tau \gg 1$) is a necessary condition for the creation of folds in the slow manifold $\Sigma_s(0)$.

For the Earth-Moon system, where m_0 is the mass of the Moon, $\epsilon = 0.0036$ and $n_o^{-1} = 7.6$ days, a value $\tau > 76$ days gives $\tilde{\epsilon} < 0.0025$. For the Mercury-Sun system, where m_0 is the mass of the Sun, $\epsilon = 6.8 \times 10^{-10}$ and $n_o^{-1} = 13$ days, a value $\tau > 130$ days gives $\tilde{\epsilon} < 0.0025$. In the case of the parameters chosen for HD80606b, $\tilde{\epsilon} \approx 1.28 \cdot 10^{-5}$.

For $\tilde{\epsilon} \ll 1$ and close to a resonance $\omega/n = j/2$, $j \in \{2, 3, \dots\}$, $\Sigma_s(0)$ can be approximately computed as a power series in ϵ . If we substitute

$$\omega/n = j/2 + \Phi(j/2, e, \tilde{\epsilon}) = j/2 + \Phi_1(j/2, e)\tilde{\epsilon} + \Phi_2(j/2, e)\tilde{\epsilon}^2 + \dots$$

into the equation

$$\sum_{k=-\infty}^{\infty} \left(X_k^{-3,2}(e) \right)^2 \frac{(\Phi(j/2, e, \tilde{\epsilon}) + (j - k)/2)}{\tilde{\epsilon} + (1 - e^2)^3 (\Phi(j/2, e, \tilde{\epsilon}) + (j - k)/2)^2} = 0, \quad (7.111)$$

and solve the resulting equation for the coefficient of $\tilde{\epsilon}$ and $\tilde{\epsilon}^2$ we obtain,

$$\Phi_1(j/2, e) = \frac{2}{(1 - e^2)^3 (X_j^{-3,2})^2} \sum_{k=1}^{+\infty} \frac{(X_{j+k}^{-3,2})^2 - (X_{j-k}^{-3,2})^2}{k}, \quad (7.112)$$

$$\begin{aligned} \Phi_2(j/2, e) &= \Phi_0(j/2, e)^3(1 - e^2)^3 \\ &+ \frac{4}{(1 - e^2)^3(X_j^{-3,2})^2} \left(\Phi_0(j/2, e) \sum_{k=1}^{+\infty} \frac{(X_{j+k}^{-3,2})^2 + (X_{j-k}^{-3,2})^2}{k^2} \right. \\ &\quad \left. + \frac{2}{(1 - e^2)^3} \sum_{k=1}^{+\infty} \frac{(X_{j-k}^{-3,2})^2 - (X_{j+k}^{-3,2})^2}{k^3} \right). \end{aligned} \quad (7.113)$$

We emphasize that the functions $\Phi(j/2, e, \tilde{\epsilon})$ represent the $\mathcal{O}(\epsilon^0)$ approximations of the slow invariant manifold $\Sigma_s(\epsilon)$. These functions determine the dynamics of the reduced system, serving as the initial step in comprehending the flow on $\Sigma_s(\epsilon)$. Further exploration of this flow constitutes a subject for future work. Figure 9 illustrates the approximation of $\Sigma_s(0)$ on some resonances.

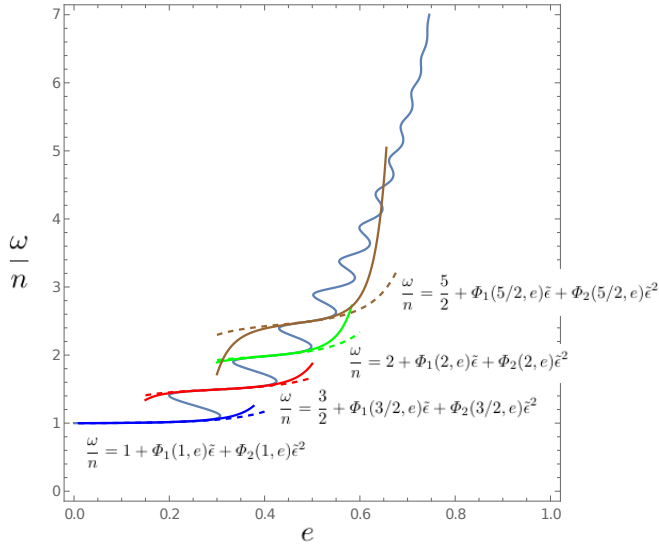


Fig. 9 Approximation of the resonances $\omega/n \approx j/2$, for $j = 2, 3, 4, 5$. The dashed lines correspond to the approximation up to $\mathcal{O}(\tilde{\epsilon})$ and the continuous lines up to $\mathcal{O}(\tilde{\epsilon}^2)$. In this graph we use the parameters of HD80606b, $\tilde{\epsilon} \approx 1.28 \cdot 10^{-5}$.

We end this section with a topological description of the slow-fast dynamics of equation (6.85). In Figure 10 we present a sketch of flow lines for $\epsilon = 0$ (LEFT panel) and $\epsilon > 0$ small (RIGHT panel). Explanations are given in the Figure caption. The orientation of the fast flow lines was previously examined in Section 6.1. The orientation of the slow flow lines is determined by the monotonic decrease in eccentricity on $\Sigma_s(0)$. This is a consequence of the same argument employed to determine the equilibria, as presented in equation (6.95).

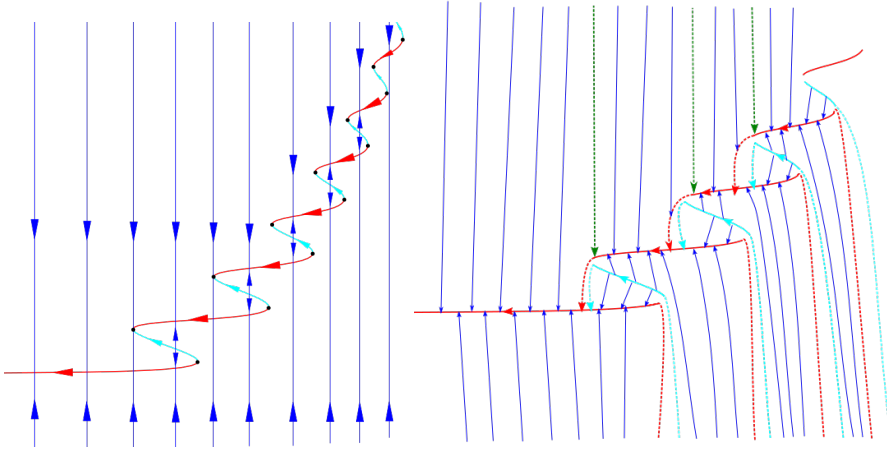


Fig. 10 The phase portrait of the averaged system (6.85). In the left, the lines in dark blue represent the solutions of the layer problem, the light blue represent the solutions of the reduced problem on the unstable branches of $\Sigma_s(0)$ and the red lines the solutions of the reduced problem on the stable branches. The black points are those at which the manifold ceases to be normally hyperbolic, the generic fold points. In the right, we depict the perturbed flow, i.e. for $\epsilon > 0$. The solutions close to the fold points, where the jumps occur, are characterized in Krupa and Szmolyan (2001a), see for instance Figure 2.1 on page 289. The perturbed fast flow is also represented in dark blue, except for some especial solutions. We highlight, in dark green, the solutions incident on the fold points, these solutions delimit the basin of attraction of the various spin-orbit resonances for prograde motions ($\omega > n$). In red and light blue are represented invariant manifolds that persisted under the perturbation. The continuation of these manifolds, dashed red and light blue, also delimit the portion of the resonances' basin of attraction for retrograde motions ($\omega < n$). We remark that, since the normally hyperbolic components of $\Sigma_s(0)$ are not compact, the persisting manifolds are not necessarily unique, however the qualitative behavior of the flow is the same, see Krupa and Szmolyan (2001a) for details. This geometric perspective also assists in the significant problem in tide theory concerning the probability of capture into spin-orbit resonances, such probabilities are proportional to the area of the basins of attraction.

8 Conclusion

In this paper, we presented a set of equations for the evolution of the orbital elements in the gravitational two-body problem under the influence of tides. These equations, previously obtained by other authors, were derived here through a two-step procedure. Initially, we used the fact that tidal deformations are very small to demonstrate the existence of an invariant manifold, which we have termed the deformation manifold. Although our arguments are mathematically sound, they lack the appropriate quantifiers. The second step involves averaging the equations on the deformation manifold. This step is contingent upon the first, leading to uncertainties about whether the averaged equations are mathematically coherent with the large values of τn used in Section 7. In the physics literature, employing large values of τn in the averaged equations has been common practice.

Analyzing the averaged equations mathematically presents a significant challenge due to the analytical complexity of the vector field, defined by infinite sums of Hansen coefficients, which are themselves infinite series in powers of eccentricity.

Given the scientific significance of this problem, it warrants investigation from a mathematical perspective. The geometric theory of singular perturbation, potentially incorporating multiple time scales as suggested in our companion paper [Ragazzo and Ruiz \(2024\)](#), appears to be a suitable mathematical framework to address this challenge.

Acknowledgements

C.R. is partially supported by FAPESP grant 2016/25053-8. L.R.S. is supported in part by FAPEMIG (Fundação de Amparo à Pesquisa no Estado de Minas Gerais) under Grants No. RED-00133-21 and APQ-02153-23.

Conflict of interest

On behalf of all authors, the corresponding author states that there is no conflict of interest.

References

- ME Alexander. The weak friction approximation and tidal evolution in close binary systems. *Astrophysics and Space Science*, 23:459–510, 1973.
- Gwenaél Boué and Michael Efroimsky. Tidal evolution of the Keplerian elements. *Celestial Mechanics and Dynamical Astronomy*, 131:1–46, 2019.
- Gwenaél Boué, Alexandre CM Correia, and Jacques Laskar. Complete spin and orbital evolution of close-in bodies using a Maxwell viscoelastic rheology. *Celestial Mechanics and Dynamical Astronomy*, 126(1-3):31–60, 2016.
- JR Cherniack. Computation of Hansen coefficients. *SAO Special Report*, 346, 1972.
- ACM Correia, C Ragazzo, and LS Ruiz. The effects of deformation inertia (kinetic energy) in the orbital and spin evolution of close-in bodies. *Celestial Mechanics and Dynamical Astronomy*, 130(8):51, 2018.
- Alexandre CM Correia and Ema FS Valente. Tidal evolution for any rheological model using a vectorial approach expressed in hansen coefficients. *Celestial Mechanics and Dynamical Astronomy*, 134(3):24, 2022.
- Alexandre CM Correia, Gwenaél Boué, Jacques Laskar, and Adrián Rodríguez. Deformation and tidal evolution of close-in planets and satellites using a Maxwell viscoelastic rheology. *Astronomy & Astrophysics*, 571:A50, 2014.
- George Howard Darwin. I. On the bodily tides of viscous and semi-elastic spheroids, and on the ocean tides upon a yielding nucleus. *Philosophical Transactions of the Royal Society of London*, 170:1–35, 1879.

- GH Darwin. On the secular changes in the elements of the orbit of a satellite revolving about a planet distorted by tides. *Nature*, 21(532):235–237, 1880.
- Michael Efroimsky. Bodily tides near spin–orbit resonances. *Celestial Mechanics and Dynamical Astronomy*, 112(3):283–330, 2012.
- Neil Fenichel. Persistence and smoothness of invariant manifolds for flows. *Indiana University Mathematics Journal*, 21(3):193–226, 1971.
- Neil Fenichel. Asymptotic stability with rate conditions. *Indiana University Mathematics Journal*, 23(12):1109–1137, 1974.
- Neil Fenichel. Asymptotic stability with rate conditions, ii. *Indiana University Mathematics Journal*, 26(1):81–93, 1977.
- Neil Fenichel. Geometric singular perturbation theory for ordinary differential equations. *Journal of differential equations*, 31(1):53–98, 1979.
- Sylvio Ferraz-Mello. Tidal synchronization of close-in satellites and exoplanets. a rheophysical approach. *Celestial Mechanics and Dynamical Astronomy*, 116(2):109–140, 2013.
- Sylvio Ferraz-Mello. The small and large lags of the elastic and anelastic tides - The virtual identity of two rheophysical theories. *Astronomy & Astrophysics*, 579:A97, 2015a.
- Sylvio Ferraz-Mello. Tidal synchronization of close-in satellites and exoplanets: Ii. Spin dynamics and extension to Mercury and exoplanet host stars. *Celestial Mechanics and Dynamical Astronomy*, 122:359–389, 2015b.
- Sylvio Ferraz-Mello. Planetary tides: theories. *Satellite Dynamics and Space Missions*, pages 1–50, 2019.
- Sylvio Ferraz-Mello. On tides and exoplanets. *Proceedings of the International Astronomical Union*, 15(S364):20–30, 2021.
- Sylvio Ferraz-Mello, Cristian Beaugé, Hugo A Folonier, and Gabriel O Gomes. Tidal friction in satellites and planets. The new version of the creep tide theory. *The European Physical Journal Special Topics*, 229:1441–1462, 2020.
- HA Folonier, S Ferraz-Mello, and E Andrade-Ines. Tidal synchronization of close-in satellites and exoplanets. III. tidal dissipation revisited and application to Enceladus. *Celestial Mechanics and Dynamical Astronomy*, 130(12):78, 2018.
- Yeva Gevorgyan. Homogeneous model for the TRAPPIST-1e planet with an icy layer. *Astronomy & Astrophysics*, 650:A141, June 2021. doi: 10.1051/0004-6361/202140736.
- Yeva Gevorgyan, Gwenaél Boué, Clodoaldo Ragazzo, Lucas S. Ruiz, and Alexandre C.M. Correia. Andrade rheology in time-domain. Application to Enceladus’ dissipation of energy due to forced libration. *Icarus*, 343:113610, 2020.
- Yeva Gevorgyan, Isamu Matsuyama, and Clodoaldo Ragazzo. Equivalence between simple multilayered and homogeneous laboratory-based rheological models in planetary science. *Monthly Notices of the Royal Astronomical Society*, 523(2):1822–1831, 2023.
- Peter Goldreich. Final spin states of planets and satellites. *The Astronomical Journal*, 71:1, 1966.

- William M Kaula. Tidal dissipation by solid friction and the resulting orbital evolution. *Reviews of geophysics*, 2(4):661–685, 1964.
- Martin Krupa and Peter Szmolyan. Extending geometric singular perturbation theory to nonhyperbolic points—fold and canard points in two dimensions. *SIAM journal on mathematical analysis*, 33(2):286–314, 2001a.
- Martin Krupa and Peter Szmolyan. Relaxation oscillation and canard explosion. *Journal of Differential Equations*, 174(2):312–368, 2001b.
- Jacques Laskar and Gwenaél Boué. Explicit expansion of the three-body disturbing function for arbitrary eccentricities and inclinations. *Astronomy & Astrophysics*, 522:A60, 2010.
- Augustus Edward Hough Love. *Some Problems of Geodynamics: Being an Essay to which the Adams Prize in the University of Cambridge was Adjudged in 1911*. CUP Archive, 1911.
- Valeri V Makarov and Michael Efroimsky. No pseudosynchronous rotation for terrestrial planets and moons. *The Astrophysical Journal*, 764(1):27, 2013.
- Piravonu Mathews Mathews, Thomas A Herring, and Bruce Allen Buffett. Modeling of nutation and precession: New nutation series for nonrigid Earth and insights into the Earth’s interior. *Journal of Geophysical Research: Solid Earth*, 107(B4):ETG–3, 2002.
- F Mignard. The evolution of the lunar orbit revisited. I. *The Moon and the planets*, 20(3):301–315, 1979.
- E Mishchenko. *Differential equations with small parameters and relaxation oscillations*, volume 13. Springer Science & Business Media, 2013.
- Carl D. Murray and Stanley F. Dermott. *Solar System Dynamics*. 2000.
- C Ragazzo and LS Ruiz. Dynamics of an isolated, viscoelastic, self-gravitating body. *Celestial Mechanics and Dynamical Astronomy*, 122(4):303–332, 2015.
- C Ragazzo and LS Ruiz. Tidal evolution and spin-orbit dynamics: The critical role of rheology. *To appear*, 2024.
- Clodoaldo Ragazzo. The theory of figures of Clairaut with focus on the gravitational modulus: inequalities and an improvement in the Darwin–Radau equation. *São Paulo Journal of Mathematical Sciences*, 14:1–48, 2020.
- Clodoaldo Ragazzo and LS Ruiz. Viscoelastic tides: models for use in Celestial Mechanics. *Celestial Mechanics and Dynamical Astronomy*, 128(1):19–59, 2017.
- Clodoaldo Ragazzo, Gwenaél Boué, Yeva Gevorgyan, and Lucas S Ruiz. Librations of a body composed of a deformable mantle and a fluid core. *Celestial Mechanics and Dynamical Astronomy*, 134(2):10, 2022.
- MG Rochester and DE Smylie. On changes in the trace of the Earth’s inertia tensor. *Journal of Geophysical Research*, 79(32):4948–4951, 1974.
- SF Singer. The origin of the Moon and geophysical consequences. *Geophysical Journal International*, 15(1-2):205–226, 1968.
- William Thomson. XXVII. On the rigidity of the Earth. *Philosophical Transactions of the Royal Society of London*, (153):573–582, 1863.